Confronting the minimal supersymmetric standard model with the study of scalar leptons at future linear e^+e^- colliders

Mihoko M. Nojiri,* Keisuke Fujii, and Toshifumi Tsukamoto
National Laboratory for High Energy Physics (KEK), Oho 1-1, Tsukuba, Ibaraki 305, Japan
(Received 19 June 1996)

Sleptons can easily be found at future linear e^+e^- colliders if kinematically accessible. Measurements of their masses and decay distributions would then determine MSSM parameters. This paper presents a detailed MC study of the production and decay of the lighter scalar τ lepton, $\tilde{\tau}_1$, decaying exclusively into the lightest neutralino. We found that $m_{\tilde{\tau}_1}$ and $\theta_{\tilde{\tau}}$ (the left-right mixing angle of $\tilde{\tau}$) would be measured within an error of a few percent. It is also found that $\tan\beta$ is determinable in some region of the parameter space through simultaneous studies of $\tilde{\tau}_1$- and $\tilde{e}$-pair production: the polarization measurement of the τ leptons from $\tilde{\tau}_1$ decays and the M_1, $m_{\tilde{\chi}_1^0}$ determination using $\tilde{e}_R$ pair production and decay. We also point out the possibility to determine $g_{\tilde{B}\tilde{e}_R e}$ through the measurement of the angular distribution of the $\tilde{e}_R$-pair production. The error on the coupling is expected to be comparable to its typical SUSY radiative correction, which is proportional to $\log(m_{\tilde{q}}/m_{\tilde{l}})$. The radiative correction affects M_1 and $\tan\beta$ determination, necessitating the full one-loop radiative correction to the $\tilde{e}_R$ production processes. The implication of these measurements of the MSSM parameters on selecting models of the origin of supersymmetry breaking is also discussed. [S0556-2821(96)03823-4]

PACS number(s): 14.80.Ly, 12.60.Jv, 13.10.+q, 13.88.+e

I. INTRODUCTION

The minimal supersymmetric standard model (MSSM) [1] is one of the most promising extensions of the standard model (SM). It predicts the existence of superpartners of SM particles (sparticles) below a few TeV to remove the quadratic divergence which appears in radiative corrections to the SM Higgs sector. The model is thus free from the so-called hierarchy problem inherent in any nonsupersymetric (non-SUSY) grand unified theory (GUT) models. It should also be noted that the gauge couplings unify very precisely at high energy in the MSSM, consistent with a SUSY SU(5) GUT prediction [2].

Supersymmetry is, however, not an exact symmetry of nature; instead, it should be somehow broken to give a mass difference between each particle and its superpartner. Various attempts have been made at explaining the existence of soft SUSY breaking [3,4]. Those different models of SUSY breaking lead to different relations among the soft breaking mass parameters at some high energy scale $M_{\rm SB}$; this scale could be as high as $M_{\rm Pl}$ or as low as $\sim 10^4$ GeV, depending on the models. Evolving the mass parameters with the renormalization group equation (RGE) of the model from $M_{\rm SB}$ to the weak scale $M_{\rm weak}$, one thus ends up with different sparticle mass spectra.

Precise measurements of masses and interactions of superparticles will be one of the most important physics targets once they are discovered. If the precision reaches a certain level, we will be able to test if a new particle satisfies relations predicted by supersymmetry. It will also enable us to measure SUSY-breaking mass parameters and to discriminate between models of even higher energy scale responsible for SUSY breaking.

This is indeed the case at proposed future linear e^+e^- colliders (LC's) operating at $\sqrt{s}=500$ GeV [5–8], which are designed to provide a luminosity in excess of $\mathcal{L}=30$ fb^{-1}/yr [9,5,8]. It should also be stressed that the background from W boson production to SUSY processes can be suppressed drastically thanks to the highly polarized electron beam available only at linear e^+e^- colliders [5,6].

The production and decay of the lighter chargino $\tilde{\chi}_1^-$ and scalar leptons $\tilde{e}$ and $\tilde{\mu}$ at a LC are studied extensively in previous works [9,5–8]. In particular, it has been shown by Monte Carlo (MC) simulations that some relations among soft SUSY-breaking parameters, which are predicted in minimal supergravity (MSUGRA) models, can be tested very stringently [5,6,8]. It has also been pointed out that one can verify some SUSY relations, such as that between the off-diagonal elements of the chargino mass matrix and the mass of the W boson or that between gauge boson-fermion-fermion and gaugino-sfermion-fermion couplings [7].

In this paper, we discuss production and decay of scalar leptons $\tilde{\tau}$ and $\tilde{e}_R$, and show how various MSSM parameters can be measured from their production only.

The $\tilde{\tau}$ is a very interesting object to study, since its mass parameters depend very sensitively on physics at the GUT scale ($M_{\rm GUT}$) [10]. In SUSY-GUT models the $\tilde{\tau}$ is in the same multiplet with $\tilde{t}$ above $M_{\rm GUT}$. Therefore the $\tilde{\tau}$ is expected to have a very large coupling, proportional to the top Yukawa coupling, to color triplet Higgs bosons predicted in GUT models. Even though all sfermions have equal mass at $M_{\rm Pl}$ in MSUGRA models, the large Yukawa coupling reduces the $\tilde{\tau}$ mass at $M_{\rm GUT}$ compared to those of the other scalar leptons, which might be regarded as a signature of quark-lepton unification at the GUT scale. This observation implies that the stau can be found earlier than the other charged sleptons, which is also phenomenologically interesting.

*Electronic address: nojirim@theory.kek.jp

In order to obtain the GUT scale mass parameters, one has to evolve the mass parameters at $M_{\rm weak}$ toward $M_{\rm GUT}$. This requires knowledge not only of the $\tilde{\tau}$ mass matrix at $M_{\rm weak}$, but also of the weak scale τ Yukawa coupling $Y_\tau = -g m_\tau/(\sqrt{2} m_W \cos\beta)$, which is determined by the ratio of vacuum expectation values $\tan\beta$. Y_τ may have very large effects on the RG running of $m_{\tilde{\tau}_1}$ for $\tan\beta \sim 50$: Such a large value of $\tan\beta$ is expected in a minimal SO(10) GUT model [11].

The measurement of Y_τ is known to be difficult [5], but it has been pointed out [12,13] that the decay distribution of $\tilde{\tau}$ contains some information on this coupling.

$\tilde{\tau}$ production and decay are different from $\tilde{e}$ or $\tilde{\mu}$, because of the non-negligible τ Yukawa coupling involved in their mass matrix and interactions. Because of this coupling, $\tilde{\tau}_R$ and $\tilde{\tau}_L$ mix, and the mass eigenstates are not necessarily current eigenstates. The same Yukawa coupling appears as a non-negligible $\tau\tilde{\tau}\tilde{H}_1^0$ coupling, where $\tilde{H}_1^0$ is a neutral Higgsino. This interaction is involved in $\tilde{\tau}$ decay into a neutralino ($\tilde{\chi}_i^0$) and τ or a chargino($\tilde{\chi}_i^-$) and ν_τ, since the $\tilde{\chi}$'s are mixtures of Higgsinos and gauginos.

Another feature of $\tilde{\tau}$ decay that distinguishes it from other slepton decays is that the daughter τ lepton from the decay $\tilde{\tau} \to \tilde{\chi}_i^0 \tau$ further decays in the detector, which enables us to measure the average polarization of the τ [$P_\tau(\tilde{\tau} \to \tau\tilde{\chi})$] [14]. The τ lepton from $\tilde{\tau}_1$ decay is naturally polarized. The polarization P_τ in the decay $\tilde{\tau}_1 \to \tilde{\chi}_i^0 \tau$ depends on Y_τ. This dependence arises because the interaction of gauginos with (s)fermions preserves chirality and is proportional to a gauge coupling, while the interaction of Higgsinos flips chirality and is proportional to Y_τ. P_τ from decaying $\tilde{\tau}_1$ reflects the ratio of the chirality flipping and conserving interactions and is therefore sensitive to Y_τ.

P_τ also depends on the $\tilde{\tau}$ left-right mixing angle $\theta_{\tilde{\tau}}$ and on the neutralino mixing N_{ij}, which in turn depends on $(M_1, M_2, \mu, \tan\beta)$. $\theta_{\tilde{\tau}}$ can be determined independently from a measurement of the $\tilde{\tau}$ pair production cross section. On the other hand, information on N_{ij} must be obtained elsewhere, for example, from $\tilde{e}_R$ pair production and decay. Selectron pair production involves t-channel exchange of neutralinos. By studying $\tilde{e}_R$ pair production followed by the decay $\tilde{e}_R \to e\tilde{\chi}_1^0$, one can thus not only measure the mass of the $\tilde{\chi}_1^0$ ($m_{\tilde{\chi}_1^0}$), but also very strongly constrain the gaugino mass parameter M_1. Making use of the measured $P_\tau(\tilde{\tau} \to \tau\tilde{\chi}_1^0)$ and assuming a GUT relation between M_1 and M_2, we can in principle determine all the parameters of the neutralino mass matrix: M_1, μ, and $\tan\beta$. One purpose of this paper is to reveal the feasibility of the $\tan\beta$ measurement at future LC's.

Another aspect of the $\tilde{e}_R$ and $\tilde{\tau}_1$ measurements is also treated in this paper. In the high energy limit, $\tilde{e}_R$ production involves s-channel exchange of the $\mathrm{U}(1)_Y$ gauge boson B and t-channel exchange of its superpartner $\tilde{B}$. The process turns out to provide clear information on the $\tilde{B}$-e_R-$\tilde{e}_R$ coupling $g_{\tilde{B}\tilde{e}_R e_R}$. Assuming that the $\tilde{e}_R$ angular distribution can be reconstructed from that of daughter electrons, we find that the sensitivity to the coupling $g_{\tilde{B}e_R\tilde{e}_R}$ would reach $\sim 1\%$ (which corresponds to a few percent sensitivity to the production cross section). The sensitivity is then comparable to the typical radiative correction to the SUSY relation $g_{\tilde{B}e_R\tilde{e}_R} = \sqrt{2} g'$, which is proportional to $\log(m_{\tilde{q}}/m_{\tilde{l}})$. This is the first example where radiative corrections to couplings involving superpartners might be measured experimentally.

We also discuss what the $P_\tau(\tilde{\tau} \to \tau\tilde{\chi}_1^0)$ measurement implies in the limit where $\tilde{\chi}_1^0$ is dominantly gaugino. In this limit, the sensitivity to $\tan\beta$ disappears since no $\tilde{\tau}\tau\tilde{H}_1^0$ interaction is involved in the $\tilde{\tau}\tau\tilde{\chi}_1^0$ coupling. However, in this case, we show that sensitivity to the chiral nature of $\tilde{\tau}\tau\tilde{B}$ coupling emerges, offering another test of a supersymmetry relation.

The organization of this paper is as follows. In Sec. II we review the physics involved in the $\tilde{\tau}_1$ mass matrix. In Sec. II A, we describe the relation between the weak scale parameters $m_{\tilde{\tau}_1}$, $m_{\tilde{\tau}_2}$, and $\theta_{\tilde{\tau}}$ and GUT scale $\tilde{\tau}$ mass matrices in detail. The importance of measuring $\theta_{\tilde{\tau}}$ and $\tan\beta$ is stressed there, since it allows us to check the relation between $m_{\tilde{e}}$ and $m_{\tilde{\tau}}$ at $M_{\rm GUT}$. Section II B is devoted to describing the procedure to determine $\tan\beta$ from the measurements of $P_\tau(\tilde{\tau} \to \tau\tilde{\chi})$ and of $\tilde{e}_R$ pair production. In Sec. II C, we discuss the energy distribution of $\tilde{\tau}$ decay products, from which $P_\tau(\tilde{\tau} \to \tau\tilde{\chi})$ and $m_{\tilde{\tau}_1}$ are measured.

Our MC studies of $\tilde{\tau}$ pair production and decay are described in detail in Sec. III, where one can find our error estimates on $m_{\tilde{\tau}}$, $\theta_{\tilde{\tau}}$, and P_τ for $\int \mathcal{L} dt = 100\ \mathrm{fb}^{-1}$. Some preliminary studies have been given in proceedings reports [13], where the effects of the $e^+e^-\tau^+\tau^-$ background were not properly taken into account. In this paper, we present our final results with an optimized set of cuts to remove the background, while minimizing acceptance distortion for parameter fitting. These cuts are detailed in Sec. III A. The results of the fitting are discussed in Sec. III B.

In Sec. IV A, we define a function called $\Delta\overline{\chi^2}$, which allows convenient estimates of errors on MSSM parameters that could be obtained through fits of $\tilde{\tau}$ and $\tilde{e}$ decay distributions. Section IV B is devoted to the $\tan\beta$ determination from a simultaneous fit of $\tilde{\tau}_1$ and $\tilde{e}_R$ production using $\Delta\overline{\chi^2}$, demonstrating a unique opportunity to measure $\tan\beta$ if it is large. In Sec. IV C, we go further to determine $\tilde{e}(\tilde{\tau})$ coupling to neutralinos. Section V then summarizes our results and concludes this paper.

II. PHYSICS OF $\tilde{\tau}_1$

A. Origin of supersymmetry breaking and the mass of $\tilde{\tau}$

$\tilde{\tau}_{L(R)}$ is the superpartner of $\tau_{L(R)}$, the third generation lepton. This makes $\tilde{\tau}$ a unique object in the context of SUGRA-GUT models [10].

In minimal supergravity models, SUSY breaking in a hidden sector induces a universal soft breaking mass m_0, a universal gaugino mass M_0, and a universal trilinear coupling A_0 through gravitational interactions at the Planck scale $M_{\rm Pl}$. If the soft breaking masses remain universal from $M_{\rm Pl}$ through $M_{\rm GUT}$, this boundary condition results in the universality at the weak scale of sfermion soft breaking masses within the same representation of the $\mathrm{SU}(3) \times \mathrm{SU}(2) \times \mathrm{U}(1)_Y$ gauge interactions in the MSSM as long as their Yukawa interactions are negligible:

$$m_{\tilde{L}}^2|_{\rm weak}=(m_0^{\rm GUT})^2+0.5(M_0^{\rm GUT})^2, \tag{1a}$$

$$m_{\tilde{R}}^2|_{\rm weak}=(m_0^{\rm GUT})^2+0.15(M_0^{\rm GUT})^2. \tag{1b}$$

Here $m_{\tilde{L}(R)}$ is the soft breaking mass of the superpartner of a left- (right-) handed lepton, and $m_0^{\rm GUT}$ and $M_0^{\rm GUT}$ are the universal scalar and gaugino masses at $M_{\rm GUT}$. The model also predicts the following relations among gaugino soft breaking mass parameters:

$$M_1=\frac{5\alpha_1}{3\alpha_G}M_0^{\rm GUT},\quad M_2=\frac{\alpha_2}{\alpha_G}M_0^{\rm GUT},\quad M_3=\frac{\alpha_3}{\alpha_G}M_0^{\rm GUT}, \tag{2}$$

where M_1, M_2, and M_3 are the masses of $\mathrm{U}(1)_Y$, SU(2), and SU(3) gauginos (called B-ino, W-ino, and gluino, respectively). α_G is the gauge coupling at $M_{\rm GUT}$ where the α_i's unify.

Equation (1) does not apply for $\tilde{\tau}$, due to the possibly large τ Yukawa coupling allowed in MSSM. The Yukawa interaction of the third generation fermions is described in the MSSM by the superpotential

$$W_Y=Y_\tau H_1 E^c L+Y_b H_1 D^c Q+Y_t H_2 U^c Q, \tag{3}$$

where H_1 (H_2) is the Higgs doublet with hypercharge $Y=-1/2$ (1/2) that gives masses to down- (up-) type fermions after $\mathrm{SU}(2)\times\mathrm{U}(1)_Y$ symmetry breaking: $\langle H_1\rangle\equiv((1/\sqrt{2})v_1,0)$ and $\langle H_2\rangle\equiv(0,(1/\sqrt{2})v_2)$. Fermion masses are thus not simply proportional to their Yukawa couplings but depend on $v_{1,2}$ as well: $Y_\tau=-gm_\tau/(\sqrt{2}m_W\cos\beta)$, where $\tan\beta\equiv v_2/v_1$. In a simple SO(10) model where all the Yukawa couplings are unified at the GUT scale, $Y_\tau\sim 1$ at $M_{\rm GUT}$ and $\tan\beta$ is predicted to be around 50 [11]. For such a large $\tan\beta$, the contribution of the τ Yukawa interaction to the RG evolution of $m_{\tilde{\tau}}$ is non-negligible. $m_{\tilde{\tau}}$ receives a negative radiative correction going down from $M_{\rm GUT}$ to $M_{\rm weak}$, leading to a mass reduction compared to $m_{\tilde{e}}$. Numerical values of the $\tilde{\tau}$ soft breaking masses at $M_{\rm weak}$ for a unified Yukawa coupling at the GUT scale $Y_{\rm GUT}=1$ can be obtained using [15]

$$m_{\tilde{L}_\tau}^2=0.53(M_0^{\rm GUT})^2-0.12m_H|_{\rm GUT}^2+0.77m|_{\rm GUT}^2, \tag{4a}$$

$$m_{\tilde{R}_\tau}^2=0.15(M_0^{\rm GUT})^2-0.23m_H|_{\rm GUT}^2+0.55m|_{\rm GUT}^2. \tag{4b}$$

Here $m|_{\rm GUT}$ is the universal soft breaking mass of sfermions, and $m_H|_{\rm GUT}$ is the soft breaking mass of Higgs bosons at $M_{\rm GUT}$, which may be different from $m|_{\rm GUT}$ in the SO(10) model.[1] One can subtract Eq. (1) from Eq. (4), after setting $m_H|_{\rm GUT}$ and $m|_{\rm GUT}$ equal to $m_0^{\rm GUT}$, to single out the maximal possible effect of the Yukawa RG running from $M_{\rm GUT}$ to $M_{\rm weak}$. The effect reduces the coefficient of $(m_0^{\rm GUT})^2$ from 1 to 0.32 for $m_{\tilde{R}_\tau}^2$ and to 0.65 for $m_{\tilde{L}_\tau}^2$.

[1]The original formula in Ref. [15] contains D-term contributions, which we have neglected here.

Yet another source of the reduction of $m_{\tilde{\tau}}$ is left-right mixing [16]. The mass matrix of a slepton flavor $(\tilde{l}_L,\tilde{l}_R)$ can be written as

$$\mathcal{M}^2=\begin{pmatrix} m_{LL}^2 & m_{LR}^2\\ m_{LR}^2 & m_{RR}^2\end{pmatrix}=\begin{pmatrix} m_{\tilde{L}}^2+m_l^2+0.27D & -m_l(A_l+\mu\tan\beta)\\ -m_l(A_l+\mu\tan\beta) & m_{\tilde{R}}^2+m_l^2+0.23D\end{pmatrix}. \tag{5}$$

Here μ is the Higgsino mass parameter, A_l is the coefficient of the soft breaking term proportional to $\tilde{l}_R^*$-$\tilde{l}_L$-H_1, and $D\equiv -m_Z^2\cos(2\beta)$. The left-right mixing element (m_{LR}^2) is negligible for the lighter generations. However, for $\tilde{\tau}$, if $\tan\beta\sim 50$, the suppression from a factor of m_τ is compensated as long as the diagonal mass parameters are $\mathcal{O}(m_W)$. The mixing is also non-negligible if $m_{\tilde{L}_\tau},m_{\tilde{R}_\tau}\ll\mu$. Mixing makes the lighter mass eigenvalue $m_{\tilde{\tau}_1}$ lighter than diagonal mass terms. The mass eigenstates and eigenvalues are expressed as

$$\begin{pmatrix}\tilde{\tau}_1\\ \tilde{\tau}_2\end{pmatrix}=\begin{pmatrix}\cos\theta_{\tilde{\tau}} & \sin\theta_{\tilde{\tau}}\\ -\sin\theta_{\tilde{\tau}} & \cos\theta_{\tilde{\tau}}\end{pmatrix}\begin{pmatrix}\tilde{\tau}_L\\ \tilde{\tau}_R\end{pmatrix}, \tag{6a}$$

$$m_{\tilde{\tau}_{1,2}}=\tfrac{1}{2}[m_{LL}^2+m_{RR}^2\mp\sqrt{(m_{LL}^2-m_{RR}^2)^2+4(m_{LR}^2)^2}], \tag{6b}$$

$$\tan\theta_{\tilde{\tau}}=\frac{m_{\tilde{\tau}_1}^2-m_{LL}^2}{m_{LR}^2}. \tag{6c}$$

$\tilde{\tau}_1$ may hence be lighter than $\tilde{e}$, even in a model with a common soft breaking sfermion mass at $M_{\rm weak}$.

We learned that determination of $\tan\beta$ characterizing the RG running of $m_{\tilde{\tau}}$ from $M_{\rm GUT}$ to $M_{\rm weak}$ and of the weak scale $\tilde{\tau}$ mass matrix parametrized by $m_{\tilde{\tau}_1},m_{\tilde{\tau}_2}$, and $\theta_{\tilde{\tau}}$ is necessary to extract $m_{\tilde{L}_\tau}$ and $m_{\tilde{R}_\tau}$ at $M_{\rm GUT}$. The values at $M_{\rm GUT}$ are interesting since they sensitively depend on the nature of quark-lepton unification, as has been emphasized recently in Ref. [10]. The reason is the following: In simple grand unified models such as supersymmetric SO(10) or SU(5) models, the $\tau_{R(L)}$ superfield is in the same multiplet as the top quark superfield above $M_{\rm GUT}$. Thus from $M_{\rm Pl}$ to $M_{\rm GUT}$, the $\tau_{R(L)}$ supermultiplet is subject to the same Yukawa interaction as the top quark. This reduces $m_{\tilde{R}_\tau}$ [and $m_{\tilde{L}_\tau}$] at $M_{\rm GUT}$ from that at $M_{\rm Pl}$ for the SU(5) [SO(10)] GUT model [10]. The reduction is predicted as a function of the top Yukawa coupling Y_t, m_0, M_0, and A_0. $m_{\tilde{R}_\tau}$ and $m_{\tilde{L}_\tau}$ could be as light as zero at $M_{\rm GUT}$ for a large value of A_0, even if $m_0^2\neq 0$.

Phenomenologically the MSUGRA-GUT suggests that $\tilde{\tau}_1$ can be the lightest charged SUSY particle, thus to be observed first, or might even be the only SUSY particle to be accessible at the first stage of proposed next generation linear e^+e^- colliders. However, we should stress that there exist models which predict totally different soft breaking mass parameters $m_{\tilde{L}_\tau,(\tilde{R}_\tau)}$. Dine, Nelson, Nir, and Shirman recently constructed a relatively simple model which dynami-

cally breaks SUSY at some intermediate scale [$\sim 10^{6-7}$ GeV] [Dine-Nelson-Nir-Shirman (DNNS) model [4]]. The breaking is then transferred to our sector by a U(1)$_Y$ gauge interaction, whose scale M_m is $\sim 10^4$ GeV. Its prediction of the gaugino mass parameters turns out to be the same as that of the MSUGRA model. This is not the case for the slepton masses, which are predicted to be common to $(\tilde{l}_L, \tilde{\nu}_l)$ and $\tilde{l}_R$, respectively, at M_m:

$$\tilde{m}_{\tilde{L}}^2 \propto \frac{3}{4}\left(\frac{\alpha_2}{4\pi}\right)^2 + \frac{5}{3}\left(\frac{1}{4}\right)^2\left(\frac{\alpha_1}{4\pi}\right)^2, \tag{7a}$$

$$\tilde{m}_{\tilde{R}}^2 \propto \frac{5}{3}\left(\frac{1}{2}\right)^2\left(\frac{\alpha_1}{4\pi}\right)^2. \tag{7b}$$

Unlike in the SUGRA-GUT model, the slepton masses do not run too much from M_m to $M_{\rm weak}$, as M_m is considerably closer to $M_{\rm weak}$ and there is no strong Yukawa interaction involved at these energy scales.[2]

The determination of $m_{\tilde{L}_\tau}$, $m_{\tilde{R}_\tau}$, and $m_{\tilde{e}(\tilde{\mu})}$ at the GUT scale would therefore give us a good handle to distinguish the MSUGRA and DNNS models or if the scale of SUSY breaking is below or above the GUT scale; it is not enough to only observe $m_{\tilde{\tau}} < m_{\tilde{e}}$, but tan$\beta$ and $\theta_{\tilde{\tau}}$ must be measured to determine $m_{\tilde{L}_\tau}$ and $m_{\tilde{R}_\tau}$ at $M_{\rm GUT}$. This shows the importance of precision studies of production and decay of $\tilde{\tau}_1$ at future LC's. We discuss in the next subsections how we can measure these parameters using $\tilde{\tau}_1$ pair production and decay.

B. Determination of MSSM mass parameters from production and decay of sleptons

Information on $\theta_{\tilde{\tau}}$ and tanβ can be extracted from the production and decay of $\tilde{\tau}$ [12,13]. In this subsection we sketch our strategy to do this. The determination of $m_{\tilde{\tau}_1}$ will be discussed in Sec. II C.

A $\tilde{\tau}$ decays into a chargino $\tilde{\chi}_i^-$ $(i=1,2)$ plus a ν_τ, or a $\tilde{\nu}_\tau$ plus a W^- or a H^-, or a neutralino $\tilde{\chi}_i^0$ $(i=1,\ldots,4)$ plus a τ. Here the neutralinos are some mixtures of the neutral components of gauginos and Higgsinos ($\tilde{B}$, $\tilde{W}$, $\tilde{H}_1^0$, and $\tilde{H}_2^0$), and the charginos are some mixtures of the charged components. Throughout this paper we assume that the lightest SUSY particle (LSP) is the lightest neutralino $\tilde{\chi}_1^0$. Because of R-parity conservation in the MSSM, the LSP is stable and escapes from detection. The decay products of any SUSY particle contain at least one $\tilde{\chi}_1^0$.

When both of the pair-produced $\tilde{\tau}_1$ decay into $\tilde{\chi}_1^0 + \tau$, the event yields a simple acoplanar $\tau^+\tau^-$ final state. If $\tilde{\tau}_1$ decays to heavier $\tilde{\chi}_i^0$ are allowed, the event might contain associated jets or leptons. Notice that if the $\tilde{\chi}_i^0$ decays into $\nu\bar{\nu}\tilde{\chi}_1^0$ the event has the same signature as that of $\tilde{\tau}_1 \to \tau\tilde{\chi}_1^0$. If one or both $\tilde{\tau}_1$'s decay into $\tilde{\chi}_i^\pm + \nu_\tau$, the event results in only one or zero τ lepton + jets or a lepton + missing momentum.

[2]Even if we take a very large Y_τ at the GUT scale, the weak scale value of Y_τ is smaller compared to that of Y_b and Y_t.

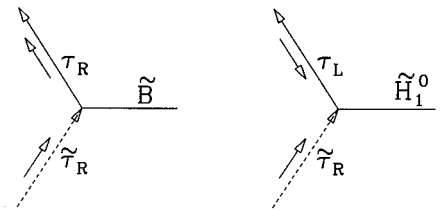

FIG. 1. Interactions of neutral components of gauginos and Higgsinos with $\tilde{\tau}_R$ and τ_L or τ_R.

The $\tilde{\tau}_1$-to-neutralino or chargino decay branching ratios depend on the scalar τ mixing $\theta_{\tilde{\tau}}$ and the parameters of the gaugino sector (M_1, (M_2), μ, tanβ). The measurement of the $\tilde{\tau}_1$ branching ratios might give us extra information on these parameters, but the existence of various decay modes also makes the analysis of $\tilde{\tau}_1$ production very complicated. This point has been discussed in previous works [12] in detail, and we will not repeat it here.

Hereafter we concentrate on the case in which the $\tilde{\tau}_R$ is the second lightest SUSY particle and decays exclusively into $\tau\tilde{\chi}_1^0$. Figure 1 shows the interactions of the neutral components of gauginos and Higgsinos with $\tilde{\tau}_R$ and τ. The interaction is completely fixed by supersymmetry. Namely, the coupling of the $\tilde{\tau}_R$ to $\tilde{B}$ is proportional to the U(1) gauge coupling g_1, while the coupling to $\tilde{H}_1^0$ is proportional to Y_τ. The two interactions have different chirality structure. The (super)gauge interaction is chirality conserving, while the (super-)Yukawa interaction flips chirality (in the figure, the arrows next to the $\tilde{\tau}$ and τ lines show flow of chirality). Since the polarization of the τ lepton $P_\tau(\tilde{\tau}_R \to \tau\tilde{\chi}_1^0)$ measures the ratio of the chirality flipping and the conserving interactions, it is sensitive to tanβ.

As we mentioned already, the gauginos and Higgsinos are not mass eigenstates, but they mix to form the neutralino mass eigenstates $\tilde{\chi}_i^0 (i=1,\ldots,4)$. The $\tilde{\tau}_R$ and $\tilde{\tau}_L$ also mix. Hence the $\tilde{\chi}_i^0\tilde{\tau}_1\tau$ couplings depend not only on tanβ but also on the stau mixing $\theta_{\tilde{\tau}}$ and the neutralino mixing N_{ij}, where N_{ij} is defined by $\tilde{\chi}_i^0 = N_{i1}\tilde{B} + N_{i2}\tilde{W} + N_{i3}\tilde{H}_1 + N_{i4}\tilde{H}_2$. Therefore, the measurement of P_τ alone cannot uniquely determine Y_τ unless $\theta_{\tilde{\tau}}$ and N_{ij} are specified. For example, in the limit where the lightest neutralino $\tilde{\chi}_1^0$ is a pure B-ino state $(N_{11} \to 1)$ and in the $\tilde{\tau}_1 \to \tilde{\tau}_{R(L)}$ limit, P_τ is expressed as

$$P_\tau(\tilde{\tau}_1 \to \tilde{B}\tau) = \frac{4\sin^2\theta_{\tilde{\tau}} - \cos^2\theta_{\tilde{\tau}}}{4\sin^2\theta_{\tilde{\tau}} + \cos^2\theta_{\tilde{\tau}}}, \tag{8a}$$

$$P_\tau(\tilde{\tau}_R \to \tilde{\chi}_1^0\tau) = \frac{(g\sqrt{2}N_{11}\tan\theta_W)^2 - (Y_\tau N_{13})^2}{(g\sqrt{2}N_{11}\tan\theta_W)^2 + (Y_\tau N_{13})^2}, \tag{8b}$$

$$P_\tau(\tilde{\tau}_L \to \tilde{\chi}_1^0\tau) = \frac{(\sqrt{2}Y_\tau N_{13})^2 - g^2(N_{12} + N_{11}\tan\theta_W)^2}{(\sqrt{2}Y_\tau N_{13})^2 + g^2(N_{12} + N_{11}\tan\theta_W)^2}, \tag{8c}$$

respectively. In the gaugino dominant limit, P_τ does not depend on tanβ as expected. On the other hand, if N_{13} is non-negligible, P_τ depends on tanβ, but how it depends differs as $\sin\theta_{\tilde{\tau}}$ varies from 0 to 1. The interactions involving $\tilde{\tau}$, $\tilde{\chi}_i^0$, and $\tilde{\chi}_i^+$ and the dependence of P_τ on these interactions

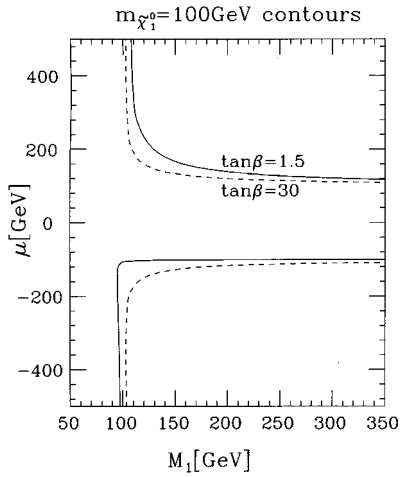

FIG. 2. $m_{\tilde{\chi}_1^0}=100$ GeV contours in the M_1-μ plane: Solid and dotted lines correspond to tan$\beta=1.5$ and 30, respectively.

are listed in Appendix A, together with the definitions of neutralino and chargino mixing angles.

Now let us turn to the determination of $\theta_{\tilde{\tau}}$ and N_{ij}.

$\tilde{\tau}_1$ Mixing angle $\theta_{\tilde{\tau}}$. Since a polarized electron beam will be available at future linear e^+e^- colliders, the mixing angle $\theta_{\tilde{\tau}}$ can be determined by the measurement of the production cross section for $e^+e^-\to\tilde{\tau}_1^+\tilde{\tau}_1^-$ [12]. This can easily be seen by taking the limit $m_Z\ll\sqrt{s}$ and $P_e=+1$. In this limit, the $\tilde{\tau}$ production solely proceeds through the exchange of the U(1)$_Y$ gauge boson B. The hypercharge for $\tilde{\tau}_{L(R)}$ is $-1/2$ (-1); thus, $\sigma(\tilde{\tau}_R)\sim 4\sigma(\tilde{\tau}_L)$. Though the cross section also depends upon $m_{\tilde{\tau}_1}$, it can be separately extracted from the energy distribution of $\tilde{\tau}$ decay products or from a threshold scan [12].

Neutralino mixing angles N_{ij} [6,13]. The neutralino mixing N_{ij} depends on M_1, M_2, μ, and tanβ. If we assume the GUT relation $M_1=5\alpha_1/(3\alpha_2)M_2$, we can determine two out of the three parameters using $\tilde{e}_R^+\tilde{e}_R^-$ pair production as we will discuss below.[3] Combining it with the $\sigma_{\tilde{\tau}\tilde{\tau}}$ and P_τ measurements, one can then determine all the parameters of the neutralino mass matrix in principle.

The $\tilde{e}_R$ pair production proceeds though the s-channel exchange of gauge bosons and the t-channel exchange of neutralinos. We list the amplitudes for the $e^+e^-\to\tilde{e}_R^+\tilde{e}_R^-$ production in Appendix B. In the limit $M_1,\mu\gg m_Z$, $\sqrt{s}\gg m_Z$, and $P_e=+1$, the amplitude reduces to

$$i\mathcal{M}\to i\beta_f g^2\tan^2\theta_W\sin\theta\left[1-\frac{4}{1-2\cos\theta\beta_f+\beta_f^2+4M_1^2/s}\right], \tag{9}$$

where θ and β_f are the polar angle and the velocity of the $\tilde{e}_R^-$. The first term in the square brackets corresponds to the s-channel exchange of gauge bosons and the second term to the t-channel $\tilde{B}$ exchange. One can see that only the interaction with the U(1)$_Y$ gauge boson (B) and the gaugino ($\tilde{B}$) is relevant in the limit, since $\tilde{e}_R$ is an SU(2) singlet.

The differential cross section $d\sigma(e^+e^-\to\tilde{e}_R^+\tilde{e}_R^-)/\cos\theta$ is very sensitive to M_1. In Ref. [6], $\tilde{e}_R^+\tilde{e}_R^-$ production and their subsequent decays $\tilde{e}_R^\pm\to e^\pm\tilde{\chi}_1^0$ have been studied in detail. It was pointed out that the three-momentum of $\tilde{e}_R$ can be derived from the momenta of the final-state electron pair with a twofold ambiguity, provided that $m_{\tilde{e}_R}$ and $m_{\tilde{\chi}_1^0}$ are known. The $\tilde{e}_R$ and $\tilde{\chi}_1^0$ masses can, on the other hand, be determined from the energy distribution of the electrons with an error of ~ 1 GeV. The study of $\tilde{e}_R$ therefore provides two out of the three parameters of the neutralino sector. The remaining freedom of tanβ can then be fixed by P_τ $(\tilde{\tau}_1\to\tau)$.

In order to illustrate how the above procedure works, we calculate the cross section contours for $e^+e^-\to\tilde{e}_R^+\tilde{e}_R^-$ and $P_\tau(\tilde{\tau}_R\to\tau\tilde{\chi}_1^0)$, fixing $m_{\tilde{\chi}_1^0}$ at 100 GeV and varying M_1 and tanβ. Curves in the M_1-μ plane which satisfy the $\tilde{\chi}_1^0$ mass constraint are shown in Fig. 2 for different values of tanβ. With the mass constraint, one can specify the position in the

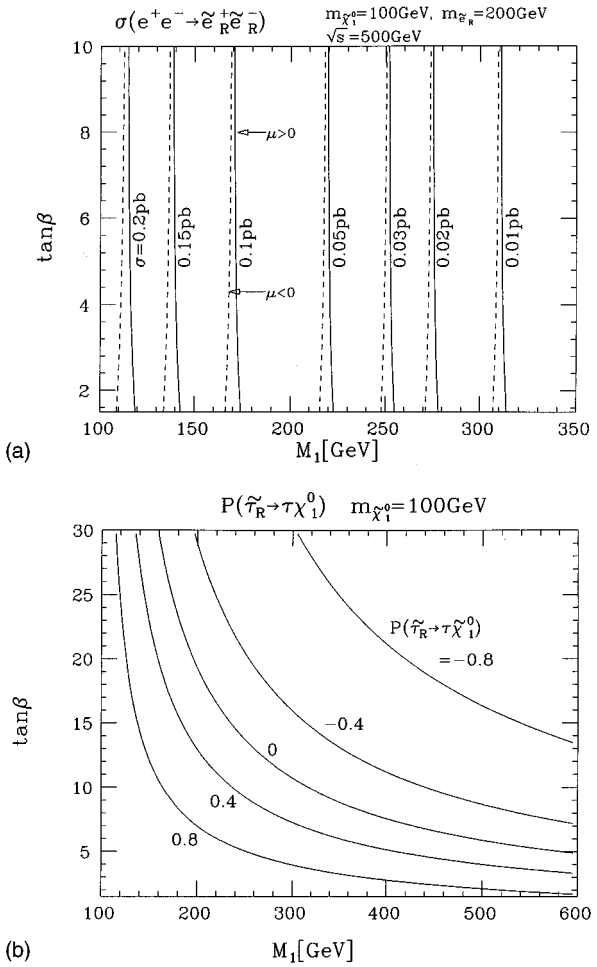

FIG. 3. (a) $\sigma_{\tilde{e}_R^+\tilde{e}_R^-}$ contours with $m_{\tilde{e}}=200$ GeV, $\sqrt{s}=500$ GeV, and $P_e=1$ in the M_1-tanβ plane. At each point of the figure, μ is chosen so that $m_{\tilde{\chi}_1^0}=100$ GeV. Solid lines correspond to a $\mu>0$ solution and the dashed lines to $\mu<0$. (b) $P_\tau(\tilde{\tau}_R\to\tau\chi_1^0)$ contours in the M_1-tanβ plane with the same neutralino mass constraint. Only the contours of $\mu>0$ solutions are shown.

[3]For any numerical calculation in this paper we assume the GUT relation, though the ratio might be determined model independently, using chargino production [6,7].

parameter space of the neutralino sector by M_1 and $\tan\beta$, up to a twofold ambiguity of positive and negative μ solutions for the large M_1 and $\tan\beta$ region or up to a threefold ambiguity of two solutions in the negative μ and one solution in the positive μ regions for small values[4] of M_1 and $\tan\beta$.

The $\sigma_{\tilde{e}_R^+\tilde{e}_R^-}$ contours corresponding to positive and negative μ solutions are shown in Fig. 3(a) as the solid and dotted lines, respectively. The difference of the two solutions is larger for smaller $\tan\beta$. For $\tan\beta>10$, the difference becomes negligible.

The dependence on $\tan\beta$ is also mild for $\sigma(e^+e^-\to\tilde{e}_R^+\tilde{e}_R^-)$, since it only comes in though the effect of the gaugino-Higgsino mixing, which is suppressed by $m_Z^2/\max(M_1,\mu)^2$ and $\sin^2\theta_W$, compared to the leading term. The effect is visible for $\tan\beta<5$ but it essentially vanishes for $\tan\beta>10$. On the other hand, the cross section is very sensitive to M_1 as expected: It decreases monotonically with increasing M_1, and turns out to be extremely small when $M_1\sim\sqrt{s}$, where the t-channel and s-channel diagrams almost cancel each other.

Figure 3(b) is a contour plot of P_τ $(\tilde{\tau}_R\to\tilde{\chi}_1^0\tau)$ in the M_1-$\tan\beta$ plane. As long as M_1 is not very close to $m_{\tilde{\chi}_1^0}$, the polarization depends on $\tan\beta$ sensitively in the region of the parameter space shown in the figure. As one can easily see from Figs. 3(a) and 3(b), if we know M_1 precisely from the $\tilde{e}_R$ production cross section, we can extract $\tan\beta$ by measuring $P_\tau(\tilde{\tau}_R\to\tilde{\chi}_1^0\tau)$ unless $M_1\sim m_{\tilde{\chi}_1^0}$. Notice when $M_1\sim m_{\tilde{\chi}_1^0}$, the lightest neutralino is gaugino dominant and there is no significant Yukawa coupling involved in P_τ as shown in Eq. (8a). Therefore we cannot expect any sensitivity to the τ Yukawa coupling in such a region of parameter space. For $M_1\gg m_{\tilde{\chi}_1^0}$, the lightest neutralino is Higgsino dominant and $\tilde{\chi}_1^0$ has significant Higgsino component. In such a case, some sensitivity to $\tan\beta$ is expected for a moderate value of $\tan\beta$ where the first and second terms of the numerator of Eq. (8b) are comparable.

Notice that in Fig. 3 we did not exclude the region forbidden by the minimal supergravity model. In MSUGRA, one has to require the square of any scalar mass parameter be positive at $M_{\rm Pl}$. This condition leads to the following inequalities at $M_{\rm weak}$: $m_{\tilde{e}_R}\gtrsim\sqrt{0.87M_1^2+0.23D}$ [see Eq. (1)]. For instance $m_{\tilde{e}_R}=200$ GeV requires $M_1<215$ GeV. If we find $M_1>215$ GeV, it will immediately bring us to conclude that the SUSY-breaking scale $M_{\rm SB}$ is much lower than $M_{\rm GUT}$, and above $M_{\rm SB}$ the theory is different from the MSSM. In the following numerical calculations, we will not assume the positivity of the scalar potential at $M_{\rm GUT}$, since the existence of models with $M_{\rm SB}\ll M_{\rm GUT}$ is not excluded. The DNNS model is an example of such a model with $M_{\rm SB}\ll M_{\rm GUT}$, although their resulting slepton and gaugino masses at the low energy scale are consistent with the positive scalar mass requirement[5] at $M_{\rm GUT}$.

[4]The ambiguities in μ might be removed for $\tan\beta<10$ by measuring other processes such as chargino production and decay.

C. Energy distribution of $\tilde{\tau}$ decay products

In this subsection, we discuss the measurements of $m_{\tilde{\tau}_1}$, $\sigma_{\tilde{\tau}\tilde{\tau}}$, and P_τ from the decay distribution of the τ leptons from the $\tilde{\tau}_1$ decays. As discussed in Secs. II A and II B, these parameters are important to determine both the $\tilde{\tau}$ mass matrix and $\tan\beta$. In Ref. [12], one of us (M.M.N.) has proposed measurements using the pion energy distribution in $\tilde{\tau}\to\tilde{\chi}_1^0\tau\to\tilde{\chi}_1^0\pi\nu_\tau$. In this paper, we discuss measurements using the decay chain $\tilde{\tau}\to\tilde{\chi}_1^0\tau\to\tilde{\chi}_1^0\rho\nu_\tau$, since we find this channel advantageous over $\tau\to\tilde{\chi}_1^0\pi\nu_\tau$, as explained below.

First consider the primary decay $\tilde{\tau}\to\tau\tilde{\chi}_1^0$. The kinematics is analogous to the $\tilde{e}$ or $\tilde{\mu}$ cases studied in Ref. [6]. The τ energy distribution is flat between the end points given by

$$E^\tau_{\max(\min)}=\frac{E^*_\tau\pm p^*_\tau\beta_{\tilde{\tau}}}{\sqrt{1-\beta^2_{\tilde{\tau}}}}, \tag{10}$$

where E^*_τ and p^*_τ are the τ energy and momentum in the parent $\tilde{\tau}$ rest frame,

$$E^*_\tau=\frac{m^2_{\tilde{\tau}}-m^2_{\tilde{\chi}_1^0}+m^2_\tau}{2m_{\tilde{\tau}}},\quad p^*_\tau=\sqrt{(E^*_\tau)^2-m^2_\tau}, \tag{11}$$

and $\beta_{\tilde{\tau}}=(1-4m^2_{\tilde{\tau}}/s)^{1/2}$ is the $\tilde{\tau}$ velocity in the laboratory frame. Knowledge of the two end point energies allows us to determine $m_{\tilde{\tau}}$ and $m_{\tilde{\chi}_1^0}$, unless $\beta_{\tilde{\tau}}$ is very close to 1.

However, the τ decays into $A\nu_\tau$, where $A=e\nu_e$, $\mu\nu_\mu$, π, ρ, a_1, etc., and $\rho^\pm$ further decays into $\pi^\pm\pi^0$ and $a_1^\pm$ to $\pi^\pm\pi^\pm\pi^\mp$ or $\pi^\pm\pi^0\pi^0$. Thus the signature of the $\tilde{\tau}^+\tilde{\tau}^-$ production is an acoplanar two-jet event with low multiplicity.

In the limit $E_\tau\gg m_\tau$, the decay products keep the original τ direction. However, the visible energy is smaller since some of the τ's energy is carried away by neutrinos. In order to determine $m_{\tilde{\tau}}$ and $m_{\tilde{\chi}_1^0}$, one must reconstruct the original τ end point energies from the energy distribution of the decay products. In Figs. 4(a) and 4(b), we show the energy distributions of the ρ and π from a decaying $\tau_{R(L)}$ with a fixed E_τ in the limit $E_\tau\gg m_\tau$ [18]. The energy distributions in the c.m. frame are obtained by convoluting these distributions with the τ energy distribution, which we show in Figs. 4(c) (for $\tilde{\tau}_1\to\tau_R^-$) and 4(d) ($\tilde{\tau}_1\to\tau_L^-$) for a representative set of parameters $m_{\tilde{\tau}_1}=150$ GeV, $m_{\tilde{\chi}}=100$ GeV, and $\sqrt{s}=500$ GeV.

[5]Another important set of constraints could be obtained from requiring the scalar potential neither be unbounded from below (UFB) nor have charge- or color-breaking (CCB) minima deeper than the standard minimum [17]. One would then find strong constraints on $m_{\tilde{\tau}_L}$ and $m_{\tilde{\tau}_R}$ at the weak scale, depending on μ and $m^2_{H_2}$. In this paper, we do not consider these constraints, since we will not specify $m_{\tilde{\tau}_2}$, $m^2_{H_2}$, and μ in the later analysis.

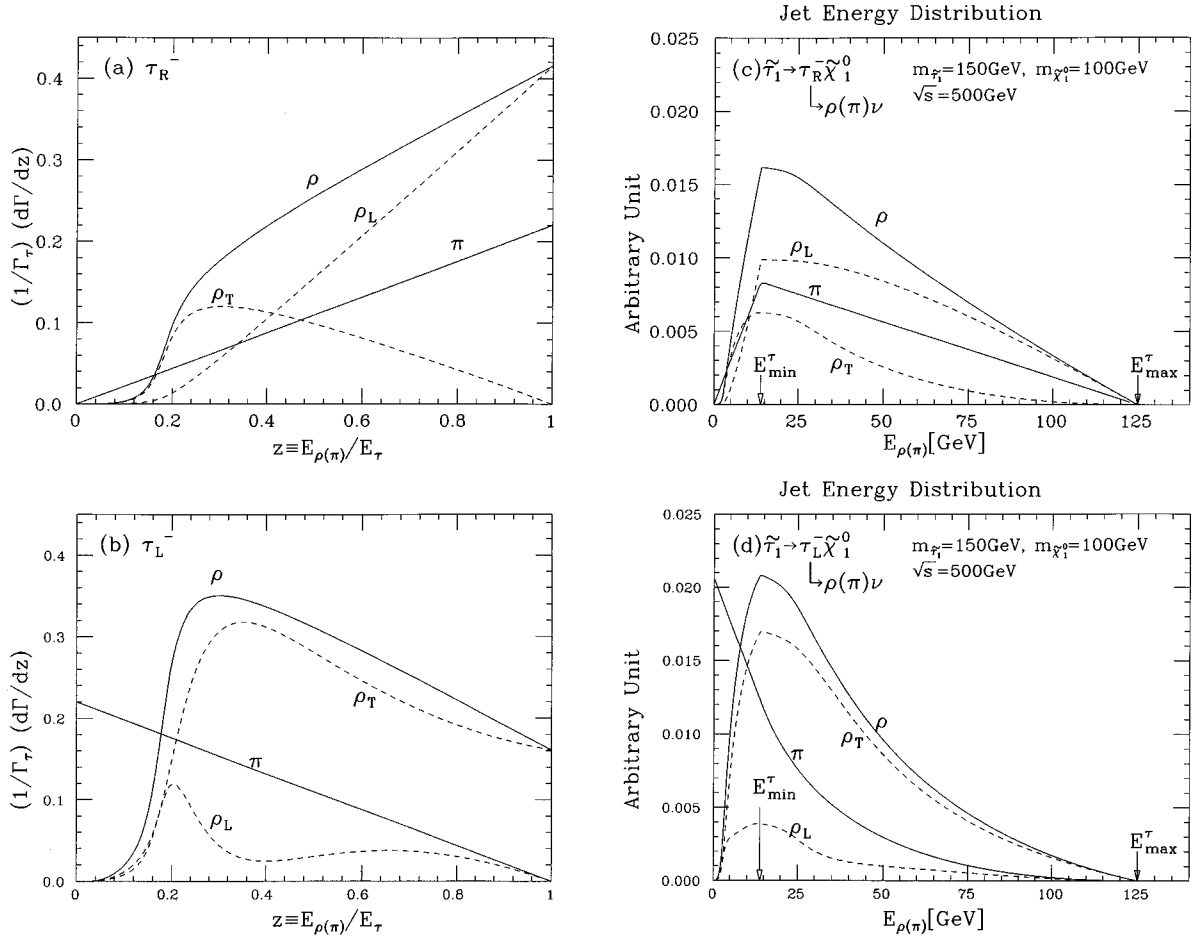

FIG. 4. (a) and (b) Energy distributions of the ρ and π from (a) τ_R decay and (b) τ_L decays with a fixed E_τ ($E_\tau \gg \tau$) as functions of $z \equiv E_{\pi(\rho)}/E_\tau$. (c) and (d) Energy distributions of the ρ and π from a cascade decay of a $\tilde{\tau}$ for $m_{\tilde{\tau}_1}$=150 GeV, $m_{\tilde{\chi}_1^0}$=100 GeV, and $\sqrt{s}$=500 GeV. The $\tilde{\tau}$ decays exclusively into $\tau^-_{R(L)}$ in (c) and (d).

The π energy distribution depends on P_τ very strongly. It is harder (softer) for a π^- from a $\tau^-_{R(L)}$ [see Figs. 4(c) and 4(d)], due to angular momentum conservation. However, a substantial correlation between P_τ and the number of identified events is expected due to the inevitable $E_{\rm vis}$ and $\not{P}_T$ cuts to remove the $e^+e^-\tau^+\tau^-$ background [9]. As we will see in Sec. III, applying these cuts drastically reduces events in lower energy region $E \lesssim E^\tau_{\rm min}$, where most of the events reside for $P_\tau \sim -1$. [The maximum and minmum energies of the original τ lepton $E^\tau_{\rm max(min)}$ are shown in Figs. 4(c) and 4(d).] If $E^\tau_{\rm min} \lesssim \not{P}^{\rm cut}_T$ it is thus hard to measure the energy distribution precisely, which results in large errors on $E^\tau_{\rm min}$ and P_τ. This uncertainty in P_τ also affects the determination of $E^\tau_{\rm max}$ as the energy distribution near $E^\tau_{\rm max}$ depends on P_τ strongly. Finally, the acceptance depends on P_τ, giving extra uncertainty in the $\tilde{\tau}_1$ total cross section measurement.

The ρ mode is preferable to the π mode in these aspects. The dependence of the energy distribution of ρ mesons on P_τ is mild, since kinematics forbids low energy ρ mesons. The energy distribution is peaked near $E^\tau_{\rm min}$ for any P_τ. The P_τ dependence of the energy distribution near $E^\tau_{\rm max}$ is also moderate. Because of this pseudo P_τ independence, we can carry out the determinations of $m_{\tilde{\tau}}$ and $(m_{\tilde{\chi}_1^0})$ and the cross section without any strong correlation to P_τ.

Furthermore, the polarization of the ρ meson depends on P_τ very strongly, which can be seen in the distributions of $\rho_{L(T)}$ in Figs. 4(c) and 4(d) (dashed lines). Namely, a τ^-_R decays mostly to a longitudinally polarized ρ meson (ρ_L) and a τ^-_L decays mostly to a transversally polarized ρ meson (ρ_T). One can thus determine P_τ by measuring P_ρ, which in turn can be determined from the distribution of the ρ decay products. A $\rho^\pm$ decays into $\pi^\pm\pi^0$, and the distribution of $E_{\pi^\pm}$ in the $\rho_{L(T)} \to \pi^\pm\pi^0$ decay is a very simple function of $z_c \equiv E_{\pi^\pm}/E_\rho$, where E_ρ is the total energy of the jet to which the $\pi^\pm$ belongs, and can be written in the form [18]

$$d\Gamma(\rho_T \to 2\pi)/dz_c \sim 2z_c(1-z_c) - 2m_\pi^2/m_\rho^2, \quad (12a)$$

$$d\Gamma(\rho_L \to 2\pi)/dz_c \sim (2z_c-1)^2, \quad (12b)$$

where we have ignored terms $O(m_\rho^2/E_\rho^2)$ but retained $O(m_\pi^2/m_\rho^2)$ contributions, and z_c is in the range $(1-\beta_\pi)/2 \le z_c \le (1+\beta_\pi)/2$, with $\beta_\pi = \sqrt{1-4m_\pi^2/m_\rho^2}$.

By fitting the z_c distribution together with the $E_{\rm jet}$ distribution, one can determine both P_τ and $m_{\tilde{\tau}_1}$. The error from

the small P_τ dependence of the $E_{\rm jet}$ distribution is reduced by the simultaneous use of the z_c distribution.

III. MONTE CARLO SIMULATIONS

A. Event selection

In this section, we investigate the feasibility of the $\tilde{\tau}$ studies outlined above at future linear e^+e^- colliders.

As discussed in the previous section, measuring the E_ρ distribution of the cascade decay $\tilde{\tau}_1 \to \tau \to \rho$ and the $z_c (\equiv E_{\pi^\pm}/E_\rho)$ distribution of the subsequent ρ decay $\rho \to \pi^\pm \pi^0$, one can determine $m_{\tilde{\tau}_1}$, P_τ, and $\theta_{\tilde{\tau}}$. However, in order to measure these parameters, one has to introduce cuts to control backgrounds. We also have to reconstruct ρ, a_1, or π from $\tilde{\tau}_1$ decays with minimum mis-ID probability among these channels. The reconstruction efficiency heavily depends on detector performance, necessitating Monte Carlo (MC) simulations with realistic detector and machine parameters. In this subsection we discuss the dominant background from $e^+e^- \to e^+e^-\tau^+\tau^-$ and present our cuts and detector setup to reduce it. We also define our cuts to identify ρ and a_1 and MC-examine the contamination due to misidentifications. The result of the fit to MC data after the cuts will be presented in Sec. III B.

In the following we study a sample case of $\tilde{\tau}_1^+\tilde{\tau}_1^-$ pair production followed by exclusive $\tilde{\tau}_1^\pm \to \tau \tilde{\chi}_1^0$ decays. We will not treat the other decay processes $\tilde{\tau}^\pm \to \tau^\pm \tilde{\chi}_i^0, (i \geq 2)$ or $\nu_\tau \tilde{\chi}_i^\pm$ where the expected event signatures are much more complicated. The helicity amplitudes for $\tilde{\tau}_1^+\tilde{\tau}_1^-$ production and their subsequent decays into $\tau\tilde{\chi}_1^0$ are calculated using the HELAS library [19]. The final state τ leptons are generated using the BASES or SPRING package [20] and are decayed with TAUOLA version 2.3 [21]. The effects of initial state radiation, beam energy spread, and beamstrahlung are also taken into account [22].

The end-product stable particles ($\pi^\pm$, γ, e, μ, . . .) are then processed through a detector simulator, and are identified, if possible, as ($\pi^\pm$,γ, . . .) candidates. In this paper, we assumed the JLC1 detector parameters, except for the forward electron veto system. The model detector is equipped with a central drift chamber [CDC: $\Delta P_t/P_t = 1.1\times 10^{-4} P_t(\text{GeV}) \oplus 0.1\%$], electromagnetic and hadron calorimeters [EMC: $\Delta E/E = 10\%/\sqrt{E(\text{GeV})} \oplus 1\%$; HDC: $\Delta E/E = 40\%/\sqrt{E(\text{GeV})} \oplus 2\%$], and muon drift chambers, whose parameters can be found in Ref. [5]. The used detector simulator is the same as the one used in the previous studies [6]. It should be noted that we tried to link charged paritcles detected in the CDC to energy clusters detected in the EMC or HDC, and when linked, we used the CDC information, since it has better resoluction in general. To be realistic in this linking process, we generated calorimeter hits with a finite shower size and simulated the cluster overlapping.

The event signatures for the $\tilde{\tau}$ pair production are acoplanar two jets or one jet + one lepton. The former mode is cleaner since the latter mode suffers from WW, $e\nu W$, and $eeWW$ backgrounds. We will, therfore, concentrate on the former mode. We used the following basic cuts to select such an acoplanar two-jet event (1) There exist two and only two jets for some $y_{\rm cut} > 2.5\times 10^{-3}$ where $y_{\rm cut}$ is imposed on the reduced jet invariant mass: $E_1E_2(1-\cos\theta_{12})/(E_{\rm vis})^2 > y_{\rm cut}$; (2) both of the two jets must clear the polar angle cut $|\cos\theta_{\rm jet}| < 0.8$; (3) the net charge of each jet must be unity and opposite in sign to that of the other; (4) the acoplanarity of the two jets has to be large enough, $\theta_{\rm acop} > 30°$; (5) these two jets have to have invariant masses consistent with τ hypothesis, $m_{\rm jet1}$, $m_{\rm jet2} < 3$ GeV; (6) the missing transverse momentum ($\not{P}_T$) has to exceed 15 GeV; (7) there has to be no electron or position above $\theta_e > 50$ mrad from the beam axis.

In addition we need cuts to identify τ decay products as ρ or a_1 in order to analyze each decay mode separately.

ρ cuts. A jet with two γ and one $\pi^\pm$ candidates is identified as a $\rho^\pm \to \pi^\pm\pi^0$ candidate if $m_{2\gamma} < 0.25$ GeV and $m_{\rm jet} < 0.95$ GeV. If there is only one γ candidate in the jet ($\gamma + \pi^\pm$), we require $m_{\rm jet} < 0.95$ GeV, assuming a possible cluster overlapping in the calorimeter.

a_1 cuts. A jet is identified as a_1 if it contains three charged π's only, or four or three γ's + one $\pi^\pm$, or two γ's + one $\pi^\pm$ with $m_{2\gamma} > 0.25$ GeV.

Cuts (1)–(4) are similar to the one used in the previous studies [6]. These cuts together with cut (5) were designed to reduce the background from gauge boson productions ($WW, e\nu W, eeWW$) to less than 1 fb for $P_e = 0.95$ at $\sqrt{s} = 500$ GeV.

Cuts (2), (4), (6), and (7) are to remove the $e^+e^- \to e^+e^-\tau^+\tau^-$ background, where the two photons radiated off from the initial-state e^+ and e^- collide to produce a τ pair, while the e^+ and e^- escape into the beam pipe.

In the previous Monte Carlo studies of the backgrounds for sfermion productions, the $e^+e^-l^+l^-$ backgrounds were eliminated by cuts on acoplanarity angle and $\not{P}_T$ [9]. The same applies to the $ee\tau\tau$ background in the $\tilde{\tau}$ production studies. One might worry about the τ decay giving extra $\not{P}_T$ to the $ee\tau\tau$ events; however, the overall reduction of the energy of the τ decay products compensates this effect. For example, at the JLC1 model detector, a $\not{P}_T > 35$ GeV cut together with an assumed electron veto angle of $\theta_e^{\rm veto} = 150$ mrad, the cuts on polar angle (cut 2), and acoplanarity angle (cut 4) turns out to remove most of the background events (Fig. 5). We have generated 110 K $e^+e^-\tau^+\tau^-$ events with $\theta_e < 150$ mrad, $E_{\tau_1} + E_{\tau_2} > 15$ GeV, $|\cos\theta_\tau| < 0.9$, and $\theta_{\rm acop} > 10°$, using a code[6] developed by Kuroda [23]. The corresponding production cross section is 1.10 pb, and therefore the generated events are about $\int \mathcal{L} dt = 100$ fb^{-1} equivalent. Twelve events survived cuts (1)–(5) and (7) and $\not{P}_T > 35$ GeV: $\sigma(ee\tau\tau)|_{\rm cut} = 0.12$ fb $\pm$ 0.035 fb. Notice that vetoing $e^\pm$'s above $\theta > 150$ mrad allows the two-photon background with the $\not{P}_T$ of the τ pair system up to as high as 75 GeV kinematically, and up to 37.5 GeV typically, since it is quite rare that the two initial-state particles give the maximum possible transverse kick in the same direction to the $\tau^+\tau^-$ system.

Introducing such a high missing P_T cut might introduce an extra correlation between the acceptance (or the measured

[6] We have generated the $e^+e^-\tau^+\tau^-$ events in the phase space sufficiently larger than the one defined by cuts (2) and (4), because the reconstructed jet axes do not in general coincide with the original τ directions.

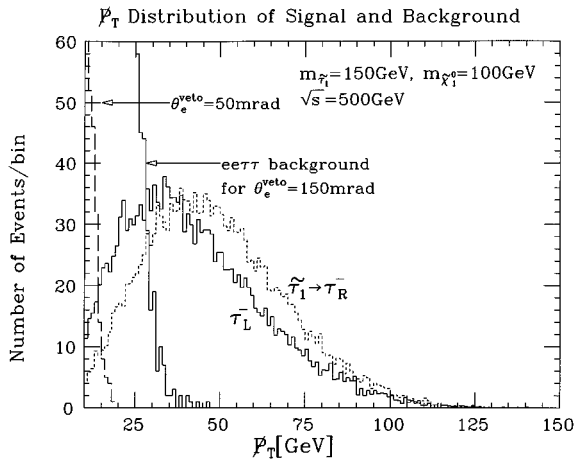

FIG. 5. $\not{P}_T$ distributions of events passing cuts (1)–(5), for $\sqrt{s}=500$ GeV, $m_{\tilde{\tau}_1}=150$ GeV, and $m_{\tilde{\chi}_1^0}=100$ GeV. The solid and dotted lines with higher $\not{P}_T$ tails are for 10^4 $\tilde{\tau}$ pairs decaying exclusively into τ_L^- and τ_R^- respectively. The $\not{P}_T$ distribution of the $ee\tau\tau$ background, also shown in the figure, corresponds to $\int \mathcal{L}dt=100$ fb^{-1}.

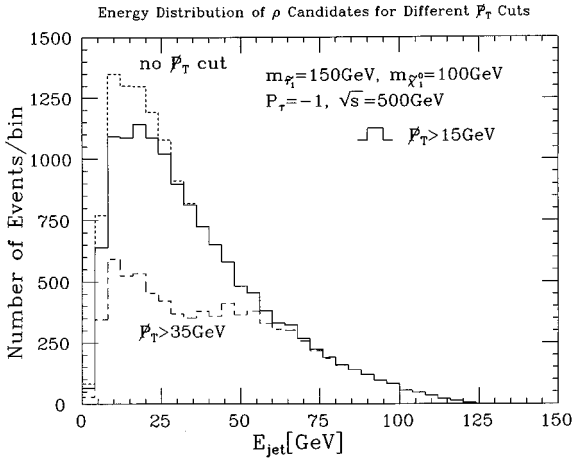

FIG. 6. $E_{\rm jet}$ distributions of 10^5 $\tilde{\tau}_1$ pairs decaying exclusively to τ_L for different total $\not{P}_T$ cuts: no $\not{P}_T$ cut (dotted line), $\not{P}_T>15$ GeV (solid line), and $\not{P}_T>35$ GeV (dashed line). $\not{P}_T>35$ GeV is the optimal cut for $\theta_e^{\rm veto}=150$ mrad, while $\not{P}_T>15$ GeV for $\theta^{\rm veto}=50$ mrad.

value of the $\tilde{\tau}$ pair production cross section) and the polarization of a τ lepton from $\tilde{\tau}_1$ decay, because jet energies become softer for a smaller $P_\tau(\tilde{\tau}\to\tau\tilde{\chi})$ as discussed already in Sec. II C. Our MC simulation for $m_{\tilde{\tau}_1}=150$ GeV, $m_{\tilde{\chi}_1^0}=100$ GeV, and $\sqrt{s}=500$ GeV shows that 17.3%($P_\tau=1$)/17.1%($P_\tau=-1$) of the generated signal events are identified as $\tilde{\tau}_1$ with no $\not{P}_T$ but $E_{\rm vis}>10$ GeV cut,[7] while only 12.6%($P_\tau=+1$)/9.8%($P_\tau=-1$) of them identified[8] for $\not{P}_T>35$ GeV. Though the correlation between P_τ and the acceptance is smaller than that of the π mode, and P_τ can also be constrained from the z_c distribution of the ρ decays, the reduction of the acceptance by up to a factor of 2 and its strong P_τ dependence might be worrisome. (See Fig. 5 for the $\not{P}_T$ distribution of the signal events corresponding to 10^4 generated $\tilde{\tau}$ pairs and the $ee\tau\tau$ background for $\int \mathcal{L}dt=100$ fb^{-1}.) It should also be noted that events with smaller jet energies are less likely to be accepted. This might complicate the simultaneous measurement of $m_{\tilde{\chi}_1^0}$ and $m_{\tilde{\tau}}$, as the measurement of the energy distribution near $E_{\rm min}^\tau$ becomes more difficult (see Fig. 6).

In this paper, we therefore assume a forward coverage down to 50 mrad. The $e^+e^-\tau^+\tau^-$ production cross section for $E_{\tau_1+\tau_2}>15$ GeV, $|\cos\theta_\tau|<0.9$, $\theta_{\rm acop}>10°$, and $\theta_e<50$ mrad is 0.719 pb. Out of 70 K generated $e^+e^-\tau^+\tau^-$ events , which correspond to $\int \mathcal{L}dt=100$ fb^{-1}, only 19 events remained as background after applying cuts (1)–(7). The overall detection efficiencies for the signal events after the same cuts are 17.0% and 16.0% for $P_\tau=1$ and $P_\tau=-1$, respectively. Jet energy distributions of ρ-identified events for different $\not{P}_T$ cuts are shown in Fig. 6 for[9] $m_{\tilde{\tau}_1}=150$ GeV, $m_{\tilde{\chi}_1^0}=100$ GeV, and $P_\tau=-1$. One can see that the $\not{P}_T>15$ GeV cut has no significant effect on the signal events as expected, while for the $\not{P}_T>35$ GeV cut, the acceptance diminishes drastically for $E_{\rm jet}<50$ GeV, making the determination of $E_{\rm min}^\tau$ difficult.

In order to realize the 50 mrad veto angle, we need to place additional veto counters in the beam background mask, which might produce extra beam backgrounds. On the other hand, having a tighter forward veto can significantly reduce the SM background in the low $\not{P}_T$ region, which will help us extend our discovery reach to SUSY particles with a mass which is very close to that of the LSP. Further studies are necessary to optimize the parameters for the extra forward electron veto. Another possibility to reduce the $\not{P}_T$ cut value is of course to go down close to the $\tilde{\tau}$ pair production threshold. If the $\tilde{\tau}$ production is accessible at $\sqrt{s}=350$ GeV, $\not{P}_T>25$ GeV must be enough to eliminate the $ee\tau\tau$ background.

Now we are going to discuss the ρ and a_1 cuts. These cuts are chosen to minimize contaminations of ρ to a_1 or vice versa due to mis-reconstruction of photons. As described earlier, the ρ and a_1 decays involve π^0's, which in turn decay into 2γ's. For a high energy π^0, however, the two photons are occasionally misidentified as a single photon due to the cluster overlapping in the calorimeter, and therefore the a_1 sometimes has the same signature as ρ. Figure 7(a) shows the jet invariant mass distributions of the events consisting of a π^- and one- or two-photon candidates coming from $\tilde{\tau}^+\tilde{\tau}^-\to\tau^+\tau^-\to\pi^+\rho^-$ and $\pi^+a_1^-$. The solid histogram is for ρ^- decays from 50 K $\tilde{\tau}$ pairs forced to decay into $\pi^+\rho^-$, and the bars are the data of 7190 $\tilde{\tau}$ pairs forced to

[7]The acceptance is smaller than that of the other sleptons since we had to require both τ's to decay hadronically. The background to the search mode where one τ decays into e/μ is larger but expected to be manageable. We also had to apply a tighter jet polar angle cut to reduce the $e^+e^-\tau^+\tau^-$ background.

[8]The P_τ dependence comes mostly from $\tilde{\tau}_1\tilde{\tau}_1\to\pi\rho$ events, where π's tend to have low energy for $P_\tau=-1$. Those events are less likely to be accepted due to the $\not{P}_T$ cut.

[9]The jet energy distributions are slightly softer than that of Fig. 4(d), as the MC simulation includes beam effects and initial-state radiation. These effects will also be included in the fits of Sec. III B.

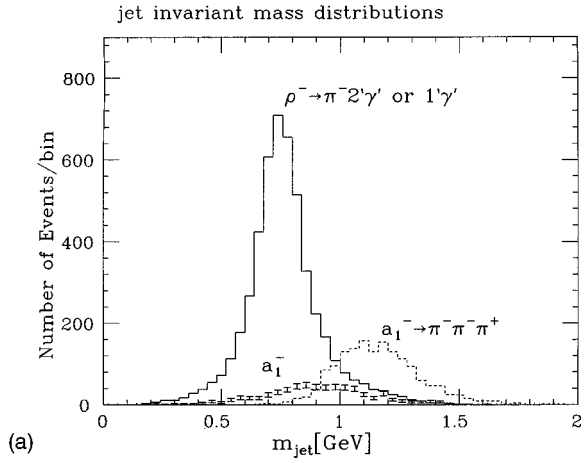

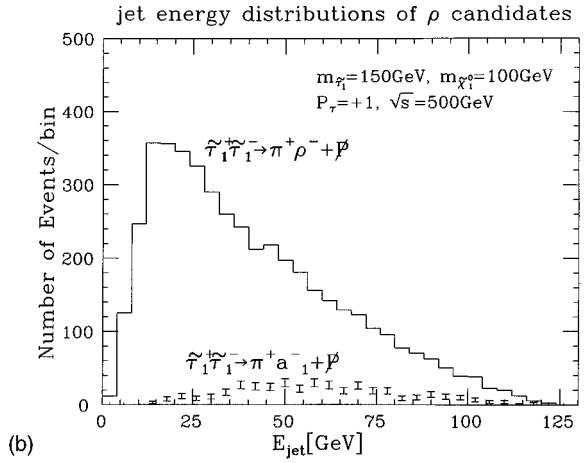

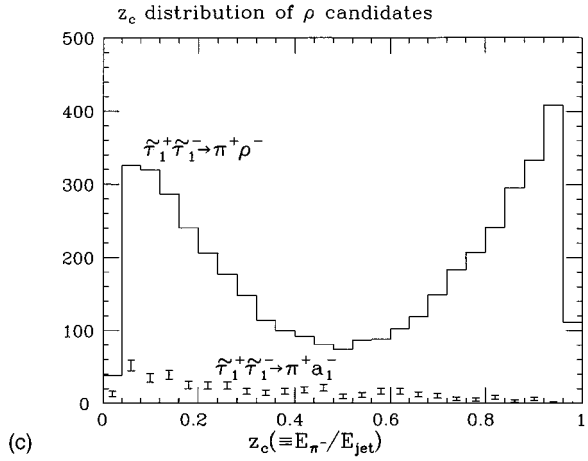

FIG. 7. (a) Invariant mass distributions of jets consisting of π^- + one or two γ's for $\tilde\tau^+\tilde\tau^- \to \tau^+\tau^-\tilde\chi_1^0\tilde\chi_1^0$, followed by $\tau^+\tau^- \to \pi^+\rho^-\nu_\tau\bar{\nu_\tau}$ (solid line) and $\pi^+ a_1^- \nu_\tau\bar{\nu_\tau}$ (bars). The latter corresponds to misidentified $a_1^- \to \pi^-\pi^0\pi^0 \to \pi^- 4\gamma$. We assumed the parameters of the JLC1 model detector. The invariant mass distribution for the jets from a_1 three-prong decays ($a_1^- \to 2\pi^-\pi^+$) is also shown as the dotted line. Because of the photon mismeasurements, the jet invariant mass distribution of a_1 one-prong decays sits below the one for three-prong decays. (b) The jet energy and (c) z_c distributions for the events that satisfy ρ cuts. The solid line is the distribution for $\tilde\tau^+\tilde\tau^- \to \pi^+\rho^-$, while bars are of $\tilde\tau^+\tilde\tau^- \to \pi^+ a_1^-$ as before. The contamination is larger for small z_c or higher E_{jet}.

decay into $\pi^+ a_1^-$. The $\pi^+\rho^-$ data are scaled so that its relative normalization to $\pi^+ a_1^-$ is correct. Because of the misreconstruction, the events have a considerably smaller jet invariant mass distribution compared to that of a_1's decaying into $2\pi^-\pi^+$(dotted histogram). The ρ cut on the invariant mass $m_{jet} < 0.95$ GeV only removes half of the a_1 contamination.

In Figs. 7(b) and 7(c), we plot the jet energy and z_c distributions of the ρ candidates that satisfy the ρ cuts in the same $\pi^+\rho^-$ and $\pi^+ a_1^-$ samples. Solid histograms are those from the $\pi^+\rho^-$ sample and bars are from the $\pi^+ a_1^-$ sample. The number of identified ρ events from $\pi^+\rho^-/\pi^+ a_1$ samples is 4522/400 for $P_\tau = +1$. The contamination is larger for a higher E_{jet} and a lower z_c. This is because high energy π^0's from a_1 decays have less chance to be identified as two photons, thereby sneaking into the ρ signals. The same MC simulation told us that very few a_1 decays could be reconstructed with $N_\gamma \geq 3$ if $E_{jet} > 50$ GeV.

The contamination affects $m_{\tilde\tau_1}$ and P_τ fit to E_{jet} and z_c distributions. In principle the a_1 contamination to the ρ sample must be corrected for before the data are fitted to obtain $m_{\tilde\tau}$ or P_τ. However, because of rather low expected statistics ($\sim$ 1400 ρ candidates expected to survive after the cuts for 10^4 $\tilde\tau$ pairs), we did not attempt to make such corrections at all. We will see in the next subsection that input parameters of MC and the corresponding best fit values of the $m_{\tilde\tau}$ and P_τ fits to $\sim 10^4$ $\tilde\tau_1$ pair events are consistent with each other.

B. Fit to MC data

In this subsection we present the results of our fits to the selected MC data for representative sets of parameters, with $m_{\tilde\tau_1} = 150$ GeV, $m_{\tilde\chi_1^0} = 100$ GeV, and $\sqrt{s} = 500$ GeV, and backgrounds for $\int \mathcal{L} dt = 100$ fb^{-1} and $P_e = 0.95$.

In Secs. II A and II B, we have discussed the importance of measuring $m_{\tilde\tau_1}$ and $\theta_{\tilde\tau}$ to determine the weak scale $\tilde\tau$ mass matrix and P_τ to determine tanβ. These parameters can be measured by looking at ρ candidates from $\tilde\tau_1$ cascade decay (Sec. II C): $m_{\tilde\tau_1}$ is measured through the energy distribution, $\sin\theta_{\tilde\tau}$ through the production cross section $\sigma_{\tilde\tau_1\tilde\tau_1}$, and P_τ through the z_c distribution.

In the following, we fit the E_{jet} and z_c distributions of the ρ candidates selected from the signal MC data to numerical functions calculated by convoluting the $\tau \to \rho_{L(T)}$ decay spectra with the τ energy distributions. The fit parameters are $m_{\tilde\tau_1}$, $m_{\tilde\chi_1^0}$, P_τ, and the number of produced $\tilde\tau_1$ pairs $N_{\tilde\tau_1\tilde\tau_1}$. The results of the fit to 10^4 and 5×10^3 $\tilde\tau_1\tilde\tau_1$ pairs will be shown in this section. Notice that the production cross section of $\tilde\tau_R(\tilde\tau_L)$ with $m_{\tilde\tau} = 150$ GeV is about 0.09 pb (0.02 pb) for $P_e = 1$; therefore, the generated 10^4 $\tilde\tau_1$ events roughly correspond to $\int \mathcal{L} dt = 100$ (400) fb^{-1}, respectively (see Fig. 1 of Ref. [12]). The fit will be extended to include the measurement of $\tilde e_R$ production and decay in Sec. IV, to obtain the error on tanβ.

We first describe our calculation of the theoretical distributions for the fit. As we mentioned earlier, the E_{jet} and/or

TABLE I. Dominant background cross sections at $P_e=+0.95$ to the process $e^+e^-\to\tilde{\tau}_1\tilde{\tau}_1$ followed by $\tilde{\tau}_1\to\tilde{\chi}_1^0\tau$. Background cross sections after requiring the cuts described in the text and the average number of ρ background events for $\int\mathcal{L}dt=100$ fb^{-1} are also shown in the table.

Process	$\sigma_{P_e=+0.95}$ (fb)	$\sigma_{\rm cut}$ (fb)	Number of ρ candidates/(100 fb^{-1})
$WW\to\tau^+\tau^-$	6.23	0.16	14.9
$eeWW\to\tau^+\tau^-$	2.16	0.21	17.9
$ZZ\to\tau^+\tau^-\nu\overline{\nu}$	4.88	0.59	51.0
$\nu\overline{\nu}Z\to\tau^+\tau^-$	0.46	0.07	6.3

z_c distributions are numerically calculated by convoluting the $\tau\to\rho_{L(T)}$ and the τ energy distributions.[10] In the calculations of the theoretical distributions, we took into account the effect of beamstrahlung and initial-state radiation on the $\tilde{\tau}_1$ energy distribution as before [22]. We also found that the acoplanarity angle cut [cut (4)] has a significant effect on the energy distribution. Since the acoplanarity angle cut is very complicated to implement in the numerical calculation of the energy distribution, we approximated the effect by imposing an acolinearity cut of 30° in the c.m. frame of the $\tilde{\tau}_1$ pairs instead. The resultant jet energy distribution that was calculated this way roughly reproduced the shape of the energy distribution of a statistically larger MC event sample (10^5 $\tilde{\tau}_1$ pairs). The overall normalization has been determined by comparing it with the MC simulation and corrected for a P_τ-dependent acceptance factor. Agreement between the z_c distribution of the MC data and that of the numerical calculation was poor for $z_c\sim0$ or $z_c\sim1$ due to the acceptance effects; we therefore fit the z_c distribution only over the range $0.08\leqslant z_c\leqslant0.92$.

In the previous subsection we have seen that the $\not{P}_T>15$ GeV cut is necessary to reduce the $ee\tau\tau$ background for an electron veto of 50 mrad. Since the signal events are hardly affected by the cut, and since it is hard to implement the $\not{P}_T$ cut in the numerical calculation of the fitting curve, we decided to ignore the $\not{P}_T$ cut for both the MC events and the fitting curve, and neglected the $ee\tau\tau$ background altogether, though the dominant backgrounds from WW, $eeWW$, ZZ, and $\nu\overline{\nu}Z$ corresponding to $\int\mathcal{L}dt=100$ fb^{-1} have been included in the fits in this section.[11] The production cross sections for the backgrounds before and after the selection cuts and the number of remaining ρ events are listed in Table I.

We first separately perform a fit of $m_{\tilde{\tau}_1}$ and $m_{\tilde{\chi}_1^0}$ to the $E_{\rm jet}$ distribution, and that of P_τ to the z_c distribution. Figures 8(a) and 8(b) are the results of our mass fit to the $E_{\rm jet}$ distribution of 10^4 $\tilde{\tau}_1\tilde{\tau}_1$ events decaying into $\tau_R\tilde{\chi}_1^0$ exclusively. Here 1476 events were identified as ρ and used for the jet energy fit. In this fit, we kept $P_\tau=+1$ and set the normalization of the curve so that the total number of events agreed with that of the MC data. Figure 8(a) plots the jet energy distribution of the MC events together with the best fit curve obtained by minimizing the log-likelihood function ($\equiv\chi^2$) with $m_{\tilde{\tau}_1}$ and $m_{\tilde{\chi}_1^0}$ as free parameters. The contours for $\Delta\chi^2=1$ and 4 in $m_{\tilde{\chi}_1^0}$-$m_{\tilde{\tau}_1}$ plane are shown in Fig. 8(b). The MC events were generated for $m_{\tilde{\tau}_1}=150$ GeV and $m_{\tilde{\chi}_1^0}=100$ GeV, while the best fit values are $m_{\tilde{\tau}_1}=147$ GeV and $m_{\tilde{\chi}_1^0}=97$ GeV for this MC sample. The values are consistent with the inputs; $\Delta m_{\tilde{\chi}_1^0}=2.8$ GeV and $\Delta m_{\tilde{\tau}_1}=3.9$ GeV can thus be expected as 1σ errors on these quantities.

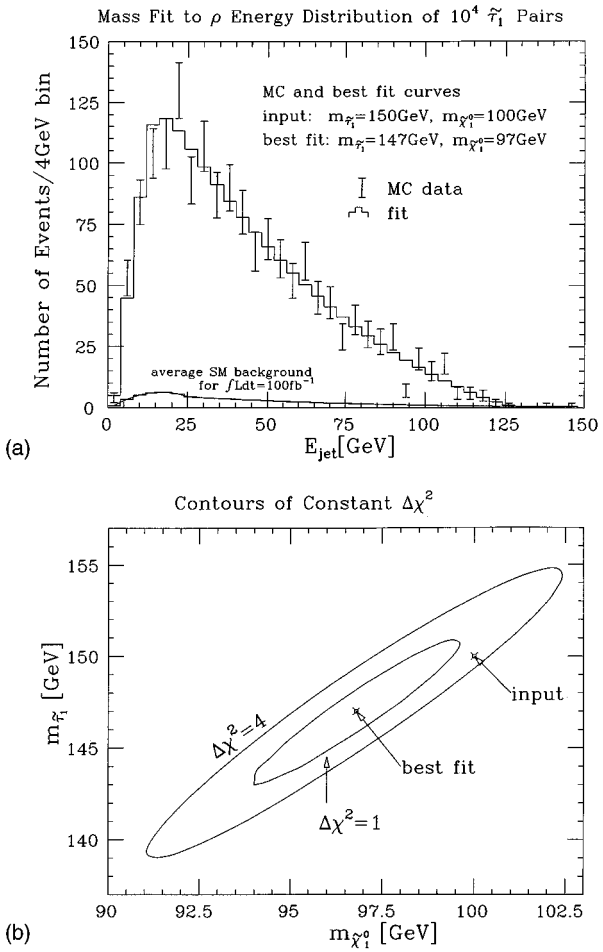

FIG. 8. Results from the mass fit to 10^4 $\tilde{\tau}_1\tilde{\tau}_1$ pair events decaying into $\tau_R\tilde{\chi}_1^0$ exclusively, where the SM background corresponding to $\int\mathcal{L}dt=100$ fb^{-1} has been included in the fit: (a) the jet energy distribution for the ρ events selected from data MC events (bars) and the best fit histogram. In the fit we kept $P_\tau=+1$ and normalized the histogram so that the total number of events agreed with that of the MC data. The average SM background is also shown in the figure. (b) Contours for $\Delta\chi^2=1$ and 4 in the $m_{\tilde{\chi}_1^0}$-$m_{\tilde{\tau}_1}$ plane.

The errors on the two parameters might be reduced further. Notice that we have only used the events identified as $\tilde{\tau}_1\to\tau\to\rho$ here. The other modes into π, a_1, or other leptons can also be used to increase the statistics. One may combine the information from other sparticle decays once they are observed. The previous analysis of $\tilde{\mu}$ decays showed that

[10]We included the effect of the finite ρ width for the jet energy distribution as in Ref. [18] but did not take it into account for the z_c distribution.

[11]$E_{\rm vis}>10$ GeV is implicit for all the MC event generation in this subsection. This condition is not included in the fitting curves as its effects were found negligible.

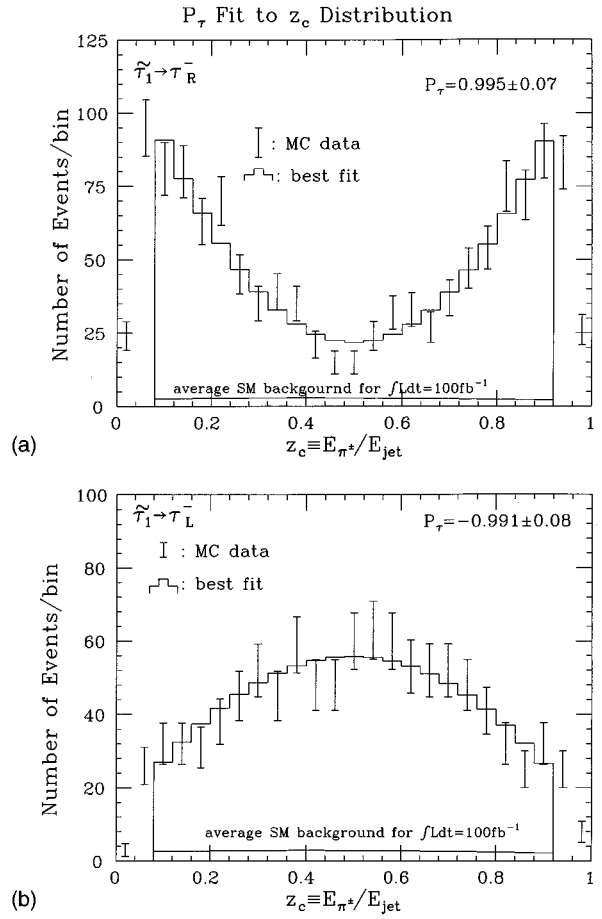

FIG. 9. z_c distributions for the ρ candidates selected from 10^4 $\tilde{\tau}_1$ pairs decaying exclusively into (a) τ_R and (b) τ_L, together with the best fit histogram. The samples with $E_{\rm jet}>20$ GeV and $0.08\leqslant z_c\leqslant 0.92$ are used for the fit. The best fit values of P_τ and their errors were obtained to be 0.995 ± 0.082 and -0.991 ± 0.008 for τ_R and τ_L, respectively, for fixed $m_{\tilde{\tau}_1}=150$ GeV and $m_{\tilde{\chi}_1^0}=100$ GeV.

$\Delta m_{\tilde{\chi}_1^0}=1$ GeV can be achieved typically, which would reduce $\Delta m_{\tilde{\tau}_1}$ down to 1.5 GeV.

On the other hand, P_τ can be determined by fitting the $\pi^\pm$ fraction of the parent ρ energy ($z_c\equiv E_{\pi^\pm}/E_{\rm jet}$). In this fit, we fixed $m_{\tilde{\chi}_1^0}$ and $m_{\tilde{\tau}_1}$ to their input values and the normalization of the fitting curve to the total number of the MC sample. Figures 9(a) and 9(b) show the z_c distribution for the selected ρ candidates together with the best fit curve. Here we used the data in the region $0.08\leqslant z_c\leqslant 0.92$ and $E_{\rm jet}>20$ GeV since the low energy region is insensitive to P_τ. Here 924(885) MC events were used for the fit where $\tilde{\tau}_1$'s decayed into $\tau_R(\tau_L)$'s. The best fit values and their errors were obtained to be 0.995 ± 0.082 and -0.991 ± 0.08 for τ_R and τ_L, respectively.

In order to justify such separate fits of $E_{\rm jet}$ and z_c distributions with some of the fitting parameters fixed by hand, we must make sure that there is no strong correlation among $m_{\tilde{\tau}_1}$, $m_{\tilde{\chi}_1^0}$, P_τ, and $\sigma_{\tilde{\tau}_1\tilde{\tau}_1}$. For this purpose, we calculated the errors on the masses and P_τ by fitting a two-dimensional distribution in $(E_{\rm jet},z_c)$, varying $m_{\tilde{\chi}_1^0}$, $m_{\tilde{\tau}_1}$, P_τ, and the total number of produced stau pair events $N_{\tau\tau}$ (which corresponds to $\sigma_{\tilde{\tau}_1\tilde{\tau}_1}$ if the integrated luminosity and acceptance is known). Here 1224 events in the interval $0.08\leqslant z_c\leqslant 0.92$ were used for the fit with $P_\tau=1$.

The resultant errors obtained from this fit agreed very well with the previous estimates. The best fit values for the masses are $m_{\tilde{\tau}_1}=146.3$ GeV and $m_{\tilde{\chi}_1^0}=95.4$ GeV. The shape of the χ^2 contour projected onto the $m_{\tilde{\chi}_1^0}$-$m_{\tilde{\tau}_1}$ plane looked quite similar to that of Fig. 8. The estimated errors are $\Delta m_{\tilde{\tau}_1}=4.07$ GeV and $\Delta m_{\tilde{\chi}_1^0}=2.99$ GeV, being consistent with the previous estimates, taking into account the difference in the number of events used for each fit. The error in P_τ was also calculated allowing $m_{\tilde{\chi}_1^0}$, $m_{\tilde{\tau}_1}$, and $N_{\tau\tau}$ to move freely in minimizing χ^2. The best fit value of P_τ is $P_\tau=0.89\pm0.07$, again consistent with the previous estimate. These results support our assumption of a small correlation between the energy distribution and P_τ for the $\tau\rightarrow\rho$ decay mode.

Finally we move on to the determination of the $\tilde{\tau}$ mixing angle $\theta_{\tilde{\tau}}$. As discussed already, our strategy is to use the measurement of the production cross section together with that of $m_{\tilde{\tau}}$. We generated 5000 $\tilde{\tau}_1$ pairs decaying into $\tau\tilde{\chi}_1^0$ with $P_\tau=0.6788$. The SM backgrounds for $\int\mathcal{L}dt=100$ fb^{-1} were also included. The ρ signal sample corresponds to $\sin\theta_{\tilde{\tau}}=0.7526$, and $m_{\tilde{\tau}_1}=150$ GeV with a B-ino dominant LSP.

We used events in the region $0.08<z_c<0.92$, which, after selection, reduced to 628 events. Since the acceptance differs by about 12% between $P_\tau=1$ and $P_\tau=-1$ due to the z_c cut,[12] we minimized χ^2 in the $N_{\tilde{\tau}_1\tilde{\tau}_1}$-$m_{\tilde{\tau}_1}$ plane, varying P_τ, $m_{\tilde{\tau}_1}$, and $m_{\tilde{\chi}_1^0}$. No significant correlation was found between $N_{\tilde{\tau}_1\tilde{\tau}_1}$ and $m_{\tilde{\chi}_1^0}$ and the estimated errors[13] are $\Delta m_{\tilde{\tau}_1}=6.6$ GeV and $\Delta\sigma_{\tilde{\tau}_1\tilde{\tau}_1}=2.2$ fb. The mass error is consistent with the previous estimate if one takes into account the difference in the numbers of produced events and the acceptances. The error on the cross section is consistent with the error simply estimated by the statistics of the accepted events.

Figure 10 plots contours of constant minimized χ^2 surfaces projected onto the $m_{\tilde{\tau}_1}$-$\sin\theta_{\tilde{\tau}}$ plane. We found $\Delta\sin\theta_{\tilde{\tau}}=0.049$. One can see that the correlation with $m_{\tilde{\tau}_1}$ makes the error large. It is possible to reduce the $\tilde{\tau}_1$ mass error by using the $m_{\tilde{\chi}_1^0}$ obtained from other measurements as was discussed earlier. $\Delta m_{\tilde{\chi}_1^0}=1$ GeV would reduce $\Delta m_{\tilde{\tau}_1}$ to 2.21 GeV, in which case the error on $\sin\theta_{\tilde{\tau}}$ is less than 0.03. However, the error cannot be less than 0.014, which is limited by the observed number of events.[14]

The $\tilde{\tau}_1$ decay process studied above is quite complicated compared to that of $\tilde{e}$ or $\tilde{\mu}$. Nevertheless, in the above dis-

[12]The data in $z_c\sim0$ or 1 can of course be used once detector performance is understood and included in the numerical calculation of fitting curves. The dependence of the acceptance to P_τ described here is purely artificial, unlike that caused by $\not{p}_T$ cuts.

[13]We assumed $\int\mathcal{L}dt=100$ fb^{-1}.

[14]Including other decay modes in the analysis would improve statistics and reduce $\Delta\theta_\tau$.

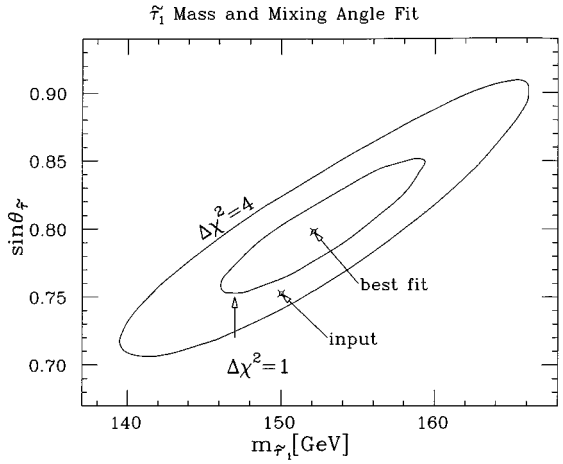

FIG. 10. $\Delta\chi^2$ contours in the $m_{\tilde{\tau}_1}$-$\sin\theta_{\tilde{\tau}}$ plane, resulting from the fit to 5000 $\tilde{\tau}_1$ pairs generated for $\int\mathcal{L}dt=100$ fb^{-1}, $m_{\tilde{\tau}_1}=150$ GeV, $m_{\tilde{\chi}_1^0}=100$ GeV, and $P_\tau=0.6788$. The MC sample corresponds to a $\tilde{\tau}_1$ with $\sin\theta_\tau=0.7526$ decaying exclusively into a B-ino-like lightest neutralino.

cussions, we have found the measurements of masses $m_{\tilde{\tau}_1}$ $m_{\tilde{\chi}_1^0}$, P_τ, and $N_{\tilde{\tau}_1\tilde{\tau}_1}$ could be done without any significant correlations each other. We have also learned that the mass errors using $\mathcal{O}(600)$ accepted ρ events are consistent with those of $\mathcal{O}(1400)$ events if the latter are statistically scaled. The error in the cross section is consistent with the error estimated by the statistics of the accepted events. This allows us to estimate the errors in $m_{\tilde{\tau}_1}$, P_τ, $N_{\tilde{\tau}\tilde{\tau}}$, and $\theta_{\tilde{\tau}}$ reliably by simple statistical scaling of each error in a wide region of parameters space. This fact is used when we combine the $\tilde{\tau}_1$ measurements with the $\tilde{e}$ measurement in the Sec. IV.

In this subsection we assumed that a tight forward electron veto is possible and applied a small $\not{P}_T$ cut as was discussed in the previous subsection. If this $\not{P}_T$ cut has to be increased to 35 GeV, the result of this subsection must change. The mass measurement is based on the measurement of $E^\tau_{\mathrm{max(min)}}$ extracted from the energy distribution of ρ candidates. As can be seen from Fig. 7, events near E^τ_{max} are not affected by the cut; therefore, $\Delta E^\tau_{\mathrm{max}}$ will not change either. E^τ_{max} is sensitive to $m_{\tilde{\tau}_1}-m_{\tilde{\chi}_1^0}$; therefore, $\Delta m_{\tilde{\tau}_1}$ obtained with $m_{\tilde{\chi}_1^0}$ from other slepton measurements will not change significantly. ΔP_τ will not be affected too much, either, since the z_c distribution is not sensitive to P_τ for $E_\rho \lesssim 20$ GeV, which is the region most affected by the $\not{P}_T > 35$ GeV cut. Finally, some extra dependence of the acceptance on P_τ should be introduced by the large $\not{P}_T$ cut. This might increase the error in the production cross section, since the acceptance moves by 20% with P_τ varying from 1 to -1. However, the dependence can be tamed by measuring P_τ from the z_c distribution.

IV. COMBINED ANALYSIS

A. $\Delta\overline{\chi^2_{\tilde{e}}}$ and $\Delta\overline{\chi^2_{\tilde{\tau}}}$ functions

In this section we are going to extract $\tan\beta$ by combining the measurements of $P_\tau(\tilde{\tau}\to\tau\tilde{\chi})$, $\sin\theta_{\tilde{\tau}}$, and the knowledge of the neutralino mass matrix obtained from the measurements of $\tilde{e}_R$ production and decay. Some MC simulation of $\tilde{e}$ production had already been carried out for a specific set of parameters [6], and we have just finished a corresponding MC analysis for $\tilde{\tau}_1$ in the previous section. It is now straightforward to perform combined fits to determine the MSSM parameters for representative points in the parameter space. Nevertheless, it is quite time consuming to do it exactly as in a real experiment.

Therefore, in this paper, we define a $\Delta\chi^2$-like function $\Delta\overline{\chi^2}$ to estimate the sensitivity of LC experiments to these SUSY parameters. As we mentioned already, we take a sample case where both $\tilde{\tau}_1$ and $\tilde{e}_R$ are produced at a future LC. The $\tilde{e}_R$ pairs are selected requiring acoplanar e^+e^- paris, while the $\tilde{\tau}_1$ pairs are taken from an acoplanar two-jet sample. Since these samples are statistically independent of each other, we define the $\tilde{e}$ and $\tilde{\tau}_1$ parts of the $\Delta\overline{\chi^2}$ functions $\Delta\overline{\chi^2_{\tilde{e}}}$ and $\Delta\overline{\chi^2_{\tilde{\tau}}}$ separately in this subsection. $\Delta\overline{\chi^2_{\tilde{e}}}$ and $\Delta\overline{\chi^2_{\tilde{\tau}}}$ are functions of two sets of input parameters: $(m_{\tilde{e}_R},M_1(M_2),\mu,\tan\beta)$ and $(m'_{\tilde{e}_R},M'_1(M_2)',\mu',\tan\beta')$ for $\Delta\overline{\chi^2_{\tilde{e}}}$ and $(m_{\tilde{\tau}_1},\theta_{\tilde{\tau}},M_1(M_2),\mu,\tan\beta)$ and $(m'_{\tilde{\tau}_1},\theta'_{\tilde{\tau}},M'_1(M'_2),\mu',\tan\beta')$ for $\Delta\overline{\chi^2_{\tilde{\tau}}}$. The $\Delta\overline{\chi^2}$ functions are defined in such a way that $\Delta\overline{\chi^2}=0$ when the two sets are equal and the projection of the hypersurface of $\Delta\overline{\chi^2}=1(,4,9,\ldots)$ to one of the parameters $(m'_{\tilde{e}_R},M'_1,\ldots)$ fixing $(m_{\tilde{e}_R},M_1,\ldots)$ roughly agrees with the $1(,2,3,\ldots)-\sigma$ error of that parameter. In this subsection, we first define $\Delta\overline{\chi^2_{\tilde{e}(\tilde{\tau})}}$ in detail, and then discuss the error on $\tan\beta$ in the next subsection. Readers who are interested only in the results can skip this subsection.

The polar angle(θ) distribution and the end point energies of electrons from $\tilde{e}_R$ decays can be measured at future LC experiments as discussed already in Sec. II B. Therefore we define $\Delta\overline{\chi^2_{\tilde{e}}}$ by using the two sets of quantities as

$$\Delta\overline{\chi^2_{\tilde{e}}}(m_{\tilde{e}_R},M_1(M_2),\mu,\tan\beta;m'_{\tilde{e}_R},M'_1(M_2)',\mu',\tan\beta') = \sum_{i=1}^{n_{\mathrm{bin}}}\frac{(n'_i-n_i)^2}{n_i}+\left(\frac{E^{e'}_{\mathrm{max}}-E^e_{\mathrm{max}}}{\Delta E^e_{\mathrm{max}}}\right)^2+\left(\frac{E^{e'}_{\mathrm{min}}-E^e_{\mathrm{min}}}{\Delta E^e_{\mathrm{min}}}\right)^2, \tag{13}$$

where n_i and n'_i are the expected numbers of events in the ith bin between $-1+2(i-1)/n_{\mathrm{bin}}\leqslant\cos\theta<-1+2i/n_{\mathrm{bin}}$ calculated for the first and second sets of input parameters $(m_{\tilde{e}_R}, M_1(M_2), \mu, \tan\beta)$ and $(m'_{\tilde{e}_R}, M'_1(M_2)', \mu', \tan\beta')$, respectively. For later use we calculated n_i assuming $\int\mathcal{L}dt=20$ (or 100) fb^{-1}, $\sqrt{s}=500$ GeV, a 27% acceptance, and $n_{\mathrm{bin}}=25$, making use of formulas for the $\tilde{e}_R$ pair production cross section listed in Appendix B. The acceptance is chosen to be a factor of 0.6 smaller compared to the value obtained by the MC simulation [6]. This is because our expression for the selectron production cross section does not include any effects of initial-state radiation, beam energy spread, and beamstrahlung.

$E^{e(')}_{\max}$ and $E^{e(')}_{\min}$ are the upper and lower end points of the energy distribution of electrons for the first (second) set of parameters. $\Delta E^e_{\max}$ and $\Delta E^e_{\min}$ are defined by

$$\Delta E^e_{\max(\min)} \equiv \sqrt{\frac{2}{N_{\rm av}}} \times E_{\rm bin}, \tag{14}$$

where $N_{\rm av} = n_{\rm total} E_{\rm bin}/(E^e_{\max} - E^e_{\min})$, with $E_{\rm bin} = 4$ GeV being a kind of bin width, and $n_{\rm total} = \sum_{i=1}^{n_{\rm bin}} n_i$.

$\Delta\overline{\chi^2_{\tilde{e}}}$ is chosen to reproduce the actual $\Delta\chi^2$ of the MC data fitted with the second set of parameters ($m'_{\tilde{e}_R}$, $M'_1(M_2)'$, μ', $\tan\beta'$) when n_i, $N_{\rm av} \gg 1$ and $n_{\rm total} \gg N_{\rm av}$. The reason is the following: If n_i's are replaced by actual data, the first term of Eq. (13) is χ^2 of the data fitted with the parameters ($m'_{\tilde{e}_R}$, $M'_1(M_2)'$, μ', $\tan\beta'$) based on Gaussian distributions. The difference between the data and n_i's divided by n_i must be small in the limit of large statistics if ($m_{\tilde{e}_R}$, $M_1(M_2)$, μ, $\tan\beta$) is the parameter set that nature has taken; therefore, the projection of the hypersurface that satisfies $\Delta\overline{\chi^2_{\tilde{e}}} = 1$ to one of the fitting parameters roughly indicates the size of $\pm 1\sigma$ deviation of the parameter from the best fit point. In this sense, we can call the first set of parameters as input parameters and the second set as fitting parameters.

The second and third terms are intended to represent the sensitivity of the electron energy distribution measurement to determine $E^e_{\max}$ and $E^e_{\min}$. As has been mentioned already, $m_{\tilde{e}_R}$ and $m_{\tilde{\chi}^0_1}$ can be determined from the end points of the energy distribution of electrons. In actual experiments, electron energies are measured by some detector with a finite energy resolution. The Japan Linear Collider (JLC1) model detector, for example, has $\sigma_E/E = 15\%/\sqrt{E} \oplus 1\%$ [5], demanding us to take into account the finite size of $E_{\rm bin} \sim 2$ GeV. Moreover, the energy distribution can also be smeared and distorted due to finite beam energy spread, beamstrahlung, initial-state radiation, and possible dependence of acceptance on electron energies. In the previous study the shape of the energy distribution and its dependence on $m_{\tilde{e}}$ and $m_{\tilde{\chi}^0_1}$ were obtained from the MC study itself, and the mass errors were estimated by actually fitting the energy distribution.

For simplicity we assume here that the energy distribution is flat between $E^e_{\max}$ and $E^e_{\min}$, while conservatively taking $E_{\rm bin} = 4$ GeV. If the average number ($N_{\rm av}$) of events in a single bin is large enough so that the fluctuation is negligible compared to $N_{\rm av}$, the central value of $E_{\max(\min)}$ is obtained as

$$E^e_{\max(\min)} = E^c_{\rm end} \pm \left(\frac{N_{\rm bin} - N_{\rm av}/2}{N_{\rm av}} \right) E_{\rm bin}, \tag{15}$$

where $E^c_{\rm end}$ is the central energy of the upper (lower) edge bin, $N_{\rm bin}$ is the number of events in it, and $N_{\rm av}$ is the average number of events in some intermediate bin. Based on the statistical error in $N_{\rm bin}$ estimated assuming a Gaussian distribution, the error on $E^e_{\max(\min)}$ is $\Delta E^e_{\min(\max)}/E_{\rm bin} = 1/\sqrt{N_{\rm bin}}$.

However, when the actual $E^e_{\max(\min)}$ is very close to a bin boundary, the fluctuation of $N_{\rm bin}$ becomes non-Gaussian. $N_{\rm bin}$ can even exceed $N_{\rm av}$ or becomes zero, making nonsense of Eq. (15) and the error estimate. Therefore in Eq. (14), we replaced $N_{\rm bin}$ by $N_{\rm av}/2$, which corresponds to the choice of binning where $E^e_{\max(\min)}$ is approximately at the center of the edge energy bin. In such a case, the fluctuation of the edge bin becomes Gaussian-like as long as $N_{\rm av}$ is large enough, thereby justifying our estimation.

Several comments are in order. One might think that the measurement of the end point energies does not fit any χ^2 analysis implying a Gaussian distribution if the energy resolution is too good and the expected numbers of the events in the edge bins are too small. In such a case the probability distribution for $E^e_{\max}$ or $E^e_{\min}$ is expected to be asymmetric, because if an event is observed in some energy bin between E_1 and E_2, selectron and neutralino masses which give $E^e_{\max} < E_1$ or $E_2 < E^e_{\min}$ are strongly disfavored. However, the number of events in a single bin is expected to be large enough in the ''precision measurement'' phase of the LC, and hence our treatment assuming a Gaussian distribution can be justified: We have checked if our treatment of $\Delta E^e_{\max(\min)}$ roughly reproduces the previous results on $\tilde{\mu}$ production and decay [6], and found that the $\Delta\overline{\chi^2}$ contours by using the last two terms of Eq. (13) but replacing $E^e_{\max(\min)}$ to $E^\mu_{\max(\min)}$ in the $m_{\tilde{\mu}}$-$m_{\tilde{\chi}^0_1}$ plane agree very well with the previous results for the same number of accepted events.

When we calculated the θ distribution or the electron energy distribution we occasionally found n_i less than 15 or $3\Delta E^e_{\max(\min)} > E_{\rm bin}/2$. In such a case, we merged the $\cos\theta$ bins or enlarged $E_{\rm bin}$. Our treatment underestimates the sensitivity compared to any log-likelihood analysis based on a Poisson distribution and therefore is conservative.

The $\Delta\overline{\chi^2}$ analysis mimics the true χ^2 fit to the θ and E_e distributions, though it neglects the correlation between the θ and E_e distributions through the total number of events: The fluctuations of the events in E_e bins have correlations with the fluctuations of n_i's, since the events must add up to an equal number in both distributions. This correlation disappears, however, in the limit where the number of events in the edge E_e bins is negligible compared to the total number of events, thereby justifying our method.

Finally, in the definition of $\Delta\overline{\chi^2_{\tilde{e}}}$, we assumed that the $\tilde{e}$ production angles are reconstructed precisely. This is not true since there is always a wrong solution of θ for each event. The wrong solutions must first be included in the θ distribution, which must then be subtracted statistically, bringing more uncertainty into our analysis. We also assumed that all the selected selectrons contribute to the determination of the production cross section, angular distribution, and masses, and will not distort the measurement due to $\tilde{e}_R$ decays into heavier neutralinos.

For $\tilde{\tau}_1$ pair production and their cascade decay $\tilde{\tau}_1 \to \tau \to \rho$, we have already discussed that it is important to measure the total cross section, P_τ from the decay distribution of the ρ decay products and $E^\tau_{\min}$ and $E^\tau_{\max}$ from the energy distribution of ρ candidates. Fits to 10^4 $\tilde{\tau}_1$ pairs have been done in Sec. III B, taking into account backgrounds corresponding to $\int \mathcal{L} dt = 100$ fb^{-1}, and the errors in $m_{\tilde{\tau}_1}$, $m_{\tilde{\chi}^0_1}$, and $N_{\tilde{\tau}_1\tilde{\tau}_1}$ have been obtained. In the following we

define the $\tilde{\tau}_1$ part of our $\Delta\chi^2$-like function $\Delta\overline{\chi^2_{\tilde{\tau}}}$ so that it reproduces the results in Sec. III B:

$$\Delta\overline{\chi^2_{\tilde{\tau}}}=\frac{(N-N')^2}{N}+\left(\frac{E^{\tau}_{\max}-E'^{\tau}_{\max}}{\Delta E^{\tau}_{\max}}\right)^2+\left(\frac{E^{\tau}_{\min}-E'^{\tau}_{\min}}{\Delta E^{\tau}_{\min}}\right)^2+\left(\frac{P_{\tau}-P'_{\tau}}{\Delta P_{\tau}}\right)^2, \quad (16)$$

where $N^{(')}$ is defined to be the sum of constant background ($N_{\rm bg}$) and the total number of signal ρ events ($N^{(')}_{\rm total}$) for which both of $\tilde{\tau}$'s decay directly into $\tilde{\chi}^0_1\tau$ and the τ's then decay hadronically. We took $N_{\rm bg}=100$. $N^{(')}_{\rm total}$ was estimated using an integrated luminosity of 100 fb^{-1}, the tree level cross section without any beam effects, and the acceptance obtained in the previous simulation with no $\not{P}_T$ cut. The branching ratio to $\tau\tilde{\chi}^0_1$ was calculated by the formula in Ref. [12]. Notice that in the region where the lightest neutralino is Higgsino like, the lighter chargino $\tilde{\chi}^-_1$ and the lightest and the second lightest neutralinos $\tilde{\chi}^0_1$ and $\tilde{\chi}^0_2$ are almost mass degenerate. Then the decay modes $\tilde{\tau}_1\to\tilde{\chi}^0_2\tau$ and $\tilde{\tau}_1\to\tilde{\chi}^-_1\nu_\tau$ generally open up, which would yield rather complicated final states with associated jets. As we have not studied the sensitivities and backgrounds to these modes, we will not include them in the study below; instead, we will simply take the number of events where both $\tilde{\tau}_1$'s decay into $\tilde{\chi}^0_1$ to estimate $N^{(')}_{\rm total}$.

The first term of Eq. (16) is intended to show the statistical significance of the total $\tilde{\tau}_1$ pair production cross section. On the other hand, the second and third terms express sensitivity to $E^{\tau}_{\max}$ and $E^{\tau}_{\min}$. We again calculate $\Delta E^{\tau}_{\max(\min)}$ using a rather simple set of formulas:

$$\Delta E^{\tau}_{\max}=4.8\sqrt{2/N_{\rm av}}E_{\rm bin}, \quad \Delta E^{\tau}_{\min}=1.8\sqrt{2/N_{\rm av}}E_{\rm bin}, \quad (17)$$

where $N_{\rm av}=E_{\rm bin}N_{\rm total}/(E^{\tau}_{\max}-E^{\tau}_{\min})$. The effect of the smearing of the energy distribution by the cascade decay of $\tilde{\tau}_1$ is taken into account by the overall factors on the right-hand side of Eq. (17). The factors are chosen so as to reproduce $\Delta m_{\tilde{\tau}_1}$ and $\Delta m_{\tilde{\chi}^0_1}$ in the previous subsection. The larger factor for $\Delta E^{\tau}_{\max}$ compared to $\Delta E^{\tau}_{\min}$ may be understood as the effect of the higher reduction of the events near $E^{\tau}_{\max}$ due to the τ decays [see Figs. 4(c) and 4(d)]. Finally, ΔP_{τ} is estimated statistically scaling the error on P_{τ} in Sec. III B:

$$\Delta P_{\tau}=0.07\times(1400/\sqrt{1400+N_{\rm bg}})/(N_{\rm total}/\sqrt{N}). \quad (18)$$

In Eq. (16), we assumed that there is no large correlation among the measurements of $N_{\tilde{\tau}_1\tilde{\tau}_1}$, $E^{\tau}_{\max(\min)}$, and P_{τ}. We also imply that errors on these parameters can be estimated by the statistical scaling of the results in Sec. III B. These features have been checked explicitly by the MC analysis in the same subsection.

B. Determination of tanβ from slepton production

We have already pointed out in Sec. II B that the simultaneous measurements of $\tilde{\tau}_1$ and $\tilde{e}_R$ productions would determine tanβ. In order to estimate its statistical error expected at a future LC, we have defined $\Delta\overline{\chi^2_{\tilde{e}(\tilde{\tau})}}$ functions in the previous subsection. $\Delta\overline{\chi^2_{\tilde{e}}}$ is a function of two sets of MSSM parameters $(m_{\tilde{e}_R},M_1,\ldots)$ and $(m'_{\tilde{e}_R},M'_1,\ldots)$. In the limit of infinite statistics, the projection of the hypersurface of $\Delta\overline{\chi^2}=1(,4,9,\ldots)$ to one of the parameters $(m'_{\tilde{e}_R},M'_1,\ldots)$ fixing $(m_{\tilde{e}_R},M_1,\ldots)$ agrees with the $1(,2,3,\ldots)\sigma$ error of that parameter obtained by using the $\cos\theta$ distribution and the end point energies of electrons from $\tilde{e}_R$ decays of real data. The definition of $\Delta\overline{\chi^2_{\tilde{\tau}}}$ is similar, but here the data used are the number of signal ρ events from $\tilde{\tau}_1\to\tilde{\chi}^0_1\tau$ followed by $\tau\to\nu_\tau\rho$, the end point energies of the τ's the $\tilde{\tau}_1$ decays, and the average τ polarization.

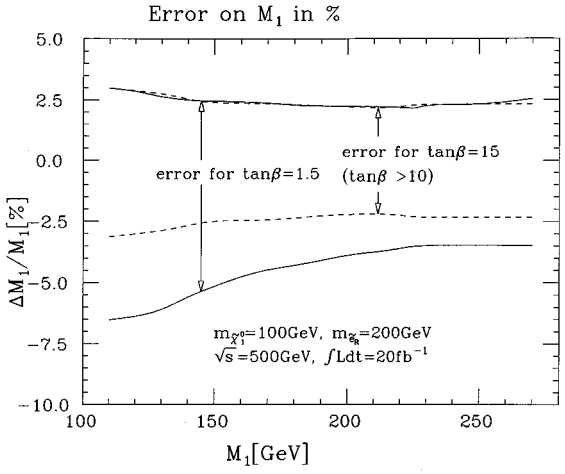

FIG. 11. 1σ error band on M_1 estimated using the $\Delta\overline{\chi^2_{\tilde{e}}}$ function. Solid and dotted lines plot values of M'_1-M_1 in percent, where $\Delta\overline{\chi^2_{\tilde{e}}}|_{\rm min}=1$ for the M'_1 varying other fitting parameters ($m'_{\tilde{e}}$, μ', tanβ'). Input values are chosen so that $m_{\tilde{\chi}^0_1}=100$ GeV and μ is positive for each M_1. Solid lines are for tan$\beta=1.5$ as input where the parameter region with $1<\tan\beta'<100$ and 50 GeV$<\mu'<10^4$ GeV was searched to obtain ΔM_1. Dashed lines for tan$\beta=15$, but only the parameter region with tan$\beta>10$ is searched to obtain these 1σ limits on M_1.

We will start our discussion with the determination of the parameters of the neutralino mass matrix from $\tilde{e}_R$ production alone. $m_{\tilde{e}_R}$ and $m_{\tilde{\chi}^0_1}$ are determined essentially by through the energy distribution of the electrons from $\tilde{e}_R$ decays. On the other hand, M_1 is mainly constrained by the $\tilde{e}_R$ production cross section. The dependence of the total cross section on M_1 and tanβ for fixed $m_{\tilde{e}_R}$ and $m_{\tilde{\chi}^0_1}$, assuming the GUT relation between M_1 and M_2, has been shown in Fig. 3(a). Notice that constraining $m_{\tilde{e}_R}$ is very important for the determination of M_1, as the production cross section depends not only on M_1 but also on $m_{\tilde{e}_R}$.

Figure 11 shows the error on M_1 estimated with the $\Delta\overline{\chi^2_{\tilde{e}}}$ function, where the input parameters were chosen such that $m_{\tilde{\chi}^0_1}=100$ GeV, $P_e=+1$, $m_{\tilde{e}_R}=200$ GeV, $\mu>0$, and $\int\mathcal{L}dt=20$ fb^{-1}. Both positive and negative errors on M_1 are shown in percent. The errors were calculated by finding a minimum value of $\Delta\overline{\chi^2}$ for a fixed $M'_1=M_1+\Delta M_1$, varying the other fitting parameters ($m'_{\tilde{e}}$,μ',tanβ'), with the MINUIT program. The values of ΔM_1 which give $\Delta\overline{\chi^2_{\rm min}}=1$ are plotted as 1σ lines in the figure. This corresponds to projecting

the $\Delta\chi^2_{\tilde{e}}=1$ hypersurface to the M_1 axis. M_1 will be determined within an error of (5–7)%, in the region of parameter space shown in the figure.[15]

We found that the errors are asymmetric for positive and negative fluctuations of M_1. This is because the condition $\Delta\chi^2=1$ forces the total cross section to be close to its input value. The cross section increases with decreasing $\tan\beta$ for $\tan\beta<5$ and decreases with increasing M_1 for fixed $m_{\tilde{\chi}^0_1}$, as can be seen in Fig. 3. For $\tan\beta=1.5$, the error on M_1 is therefore larger in the negative fluctuation (Fig. 11): Increasing $\tan\beta$ can compensate the increase of $\sigma_{\tilde{\tau}\tilde{\tau}}$ due to the reduction of M_1 here. For $\tan\beta=15$, a similar argument shows that the error is larger in the positive fluctuation.

In the figure, we have also shown the error on M_1 for $\tan\beta=15$, but restricting $\tan\beta'>10$ for searching the minimum value of $\Delta\chi^2_{\tilde{e}}$. In this case, the 1σ fluctuation is symmetric and smaller. This suggests that even a rough estimate of $\tan\beta$ can greatly help us restrict M_1. As we will see below, such an improvement is indeed possible in some region of parameter space if $\tilde{\tau}_1$ production is observed.

Now we turn to the determination of $\tan\beta$. As we have discussed already in Sec. II B, $\tan\beta$ can be extracted from the polarization of τ leptons produced in $\tilde{\tau}_1$ decays, if we know $\theta_{\tilde{\tau}}$ and the neutralino mixing angles N_{ij}.

$\theta_{\tilde{\tau}}$ is determined from the measurement of the $m_{\tilde{\tau}_1}$ and $\tilde{\tau}_1$ production cross section. (The result from our full MC analysis is in Fig. 10 in Sec. III B). The sensitivities to the production cross section, $m_{\tilde{\tau}_1}$, and P_τ are taken into account in the definition of the $\Delta\chi^2_{\tilde{\tau}}$ as the first term, the second and third terms, and the fourth term of the right-hand side of Eq. (16), respectively.

On the other hand, some information on neutralino mixing can be obtained from selectron production, e.g., by minimizing $\Delta\chi^2_{\tilde{e}}$. The neutralino mixing depends on only three (four) parameters $M_1(M_2),\mu,\tan\beta$, where $\Delta\chi^2_{\tilde{e}}$ strongly constrains two of these three parameters, M_1 and $m_{\tilde{\chi}^0_1}$, as described earlier in this subsection.

Notice that the constraint on $m_{\tilde{\chi}^0_1}$ from $\Delta\chi^2_{\tilde{e}}$ is stronger than that from $\Delta\chi^2_{\tilde{\tau}}$, because of the larger statistics of the $\tilde{e}$ production and the smearing effect of the end point energies for $E^{\tau}_{\max(\min)}$, which have been taken into account in the definition of $\Delta E^{\tau}_{\max}$ and $\Delta E^{\tau}_{\min}$ in Eq. (17). The small $\Delta m_{\tilde{\chi}^0_1}$ from the $\tilde{e}_R$ production helps determine $\tan\beta$ better, for the following reason: $\Delta m_{\tilde{\tau}_1}$ correlates with $\Delta m_{\tilde{\chi}^0_1}$ and $\Delta\theta_{\tilde{\tau}}$ with $\Delta m_{\tilde{\tau}_1}$, as can be seen in Fig. 8(b) and Fig. 10. Therefore $\Delta\theta_{\tilde{\tau}}$ is smaller for smaller $\Delta m_{\tilde{\chi}^0_1}$, which reduces the uncertainty coming from $\tilde{\tau}$ mixing in determining $\tan\beta$ from P_τ.

Figure 12 plots $\Delta\chi^2=\Delta\chi^2_{\tilde{e}}+\Delta\chi^2_{\tilde{\tau}}=1$ contours projected onto the M_1-$\tan\beta$ plane for input values of (M_1(GeV), $\tan\beta$)= (219.0,15), (149.3,15), (124.5,15), (124.5,25), and (124.5,5). The other input parameters are common for all representative points $m_{\tilde{e}}=200$ GeV, $m_{\tilde{\tau}_1}=150$ GeV, $m_{\tilde{\chi}^0_1}=100$ GeV, and $\sin\theta_{\tilde{\tau}}=1$ ($\tilde{\tau}_1=\tilde{\tau}_R$) and we took $\int\mathcal{L}dt=100$ fb^{-1}.

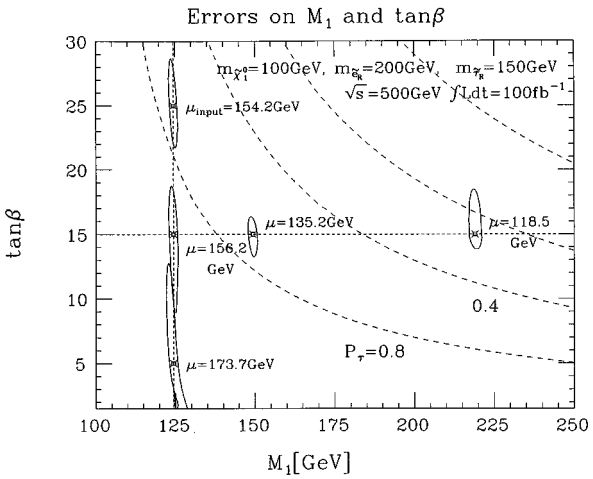

FIG. 12. $\Delta\chi^2=\Delta\chi^2_{\tilde{e}}+\Delta\chi^2_{\tilde{\tau}}=1$ contours projected onto the M_1-$\tan\beta$ plane. Projections of the contours on M_1 or $\tan\beta$ correspond to 1σ errors of the parameter. Input values are chosen to be $m_{\tilde{\tau}_1}=150$ GeV, $\sin\theta_{\tilde{\tau}}=1$ ($\tilde{\tau}_1=\tilde{\tau}_R$), $m_{\tilde{\chi}^0_1}=100$ GeV($\mu>0$), and $m_{\tilde{e}_R}=200$ GeV. Input values of μ are explicitly shown in the figure for individual sample points. $P_\tau(\tilde{\tau}_R\to\tau\tilde{\chi}^0_1)=0.8$, 0.4, 0, and -0.4 contours with $m_{\tilde{\chi}^0_1}=100$ GeV and $\mu>0$ are also plotted in the figure as dashed lines.

As we have discussed previously, P_τ depends sensitively on $\tan\beta$ if $m_{\tilde{\chi}^0_1}\ll M_1$ or $\tilde{\chi}^0_1$ is Higgsino-like, because in this case the $\chi\tilde{\tau}\tau$ coupling involves the τ Yukawa coupling. Thus the error bar is expected to be smaller for a larger M_1. However, the number of accepted events becomes small when $m_{\tilde{\chi}^0_1}\ll M_1$ because $\tilde{\tau}_1$ also decays into $\tilde{\chi}^0_2$ or $\tilde{\chi}^{\pm}_1$; therefore, the error in $\tan\beta$ for $M_1=219$ GeV is larger than that of $M_1=149.3$ GeV. When $\tan\beta=15$, the lower (upper) bounds of $\tan\beta$ for the $\Delta\chi^2=1$ contours are 13.85 (18.5), 13.28 (16.37), 8.94 (18.74) for $M_1=219$, 149.3, and 124.5 GeV, respectively.

Finally, in our definition of $\Delta\chi^2$ we did not include any luminosity error. In Ref. [5] it has been argued that the luminosity can be measured with an error of $\sim1\%$. On the other hand, using a typical $\tilde{e}$ production cross section 0.1–0.2 pb (see Fig. 2), and assuming a constant acceptance of 27%, we can see that the errors in M_1 are estimated based on ~1000 accepted $\tilde{e}$ events for the luminosity of 20 fb^{-1} (Fig. 11), and ~5000 events for 100 fb^{-1} (Fig. 12). This corresponds to an error in the cross section of about 3% and 1.4%, respectively. The latter is already comparable to the luminosity error. Hence a further increase of statistics would not improve the actual error in the MSSM parameters unless the error in the luminosity is also reduced further.

The estimated errors in $\tan\beta$ are rather impressive, compared to those from the other experimental methods. In Fig. 13, we plot the error on $\tan\beta$ which can be obtained from the lighter chargino ($\tilde{\chi}^+_1$) production and the coproduction of $\tilde{\chi}^{\pm}_1$ and $\tilde{\chi}^{\mp}_2$. Here use has been made of the direction of

[15]We found that our error on M_1 is smaller than previously quoted [6]. The previous estimate did not use the GUT relation between M_1 and M_2 and the constraint on $m_{\tilde{\chi}^0_1}$ which would have been obtained from the $\tilde{e}_R$ production was not exploited in the M_1 and M_2 fit [24]. Our result is therefore consistent with the previous one.

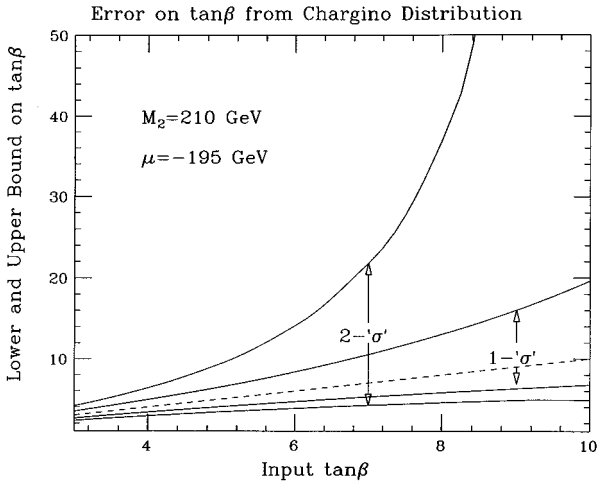

FIG. 13. 1(2)''σ'' errors on tanβ from chargino production as functions of input tanβ. We used chargino distributions for $P_e=+1$ and 0 with $\int \mathcal{L}dt=100$ fb^{-1}, and assuming that both chargino masses are known to 2% accuracy. The upper bound practically disappears when tanβ exceeds 5. Input values are $M_2=210$ GeV, $\mu=-195$ GeV, and $m_{\tilde{\nu}_2}=500$ GeV.

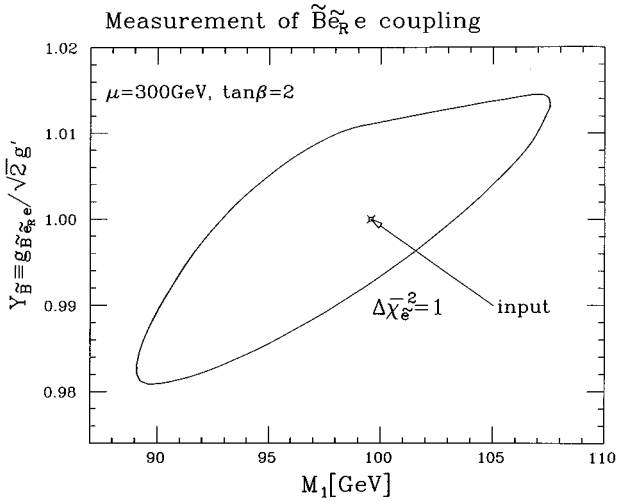

FIG. 14. $\Delta\overline{\chi^2_{\tilde{e}}}=1$ contour in the M_1-$Y_{\tilde{B}}$($\equiv g_{\tilde{B}\tilde{e}_R e}/\sqrt{2}\,g'$) plane. The definition of $\Delta\overline{\chi^2_{\tilde{e}}}$ has been modified to allow $g_{\tilde{B}\tilde{e}_R e}$ to deviate from $\sqrt{2}\,g'$. Input values are $m_{\tilde{e}_R}=200$ GeV, $\mu=300$ GeV, $M_1=99.57$ GeV, and tan$\beta=2$. The error in the coupling is of about the same order as that of the radiative correction proportional to $\log_{10}(m_{\tilde{q}}/m_{\tilde{l}})$ when $m_{\tilde{q}}/m_{\tilde{l}}\sim 10$.

pair-produced charginos $\tilde{\chi}_1^+$ with a 10% acceptance from its decay products,[16] assuming $\int \mathcal{L}dt=100$ fb^{-1} for both $P_e=1$ and 0. The errors in $m_{\tilde{\chi}_1^\pm}$ and $m_{\tilde{\chi}_2^\pm}$ were both assumed to be 2% as long as they are accessible kinematically.[17] One can see that the upper bound practically disappears[18] when tanβ exceeds 5.

C. Checking the supersymmetry relation

So far we have been assuming that new particles found at a LC are superpartners of leptons. In other words, we have implicitly been using supersymmetric interactions of sfermions with the neutralinos of the MSSM without any attempt at checking the nature of the interactions. Instead, we merely used the data to determine the free parameters of the MSSM, such as M_1 and tanβ. In this subsection we are going to discuss the possibility to probe the gaugino-sfermion-fermion interaction (more specifically, the $\tilde{B}$-$\tilde{e}_R$-e_R coupling) and some aspects of the $\tilde{B}$-$\tilde{\tau}_1$-τ coupling.

We start our discussion with $\tilde{e}_R$. The production proceeds though the s-channel exchange of gauge bosons and t-channel exchange of neutralinos, whose cross section is shown in Appendix B. The t-channel exchange is dominated by B-ino-like neutralino exchange, which led us to the simple dependence of the cross section on the gaugino mass M_1 as has been shown in Fig. 3(a).

The tree-level coupling of the $\tilde{B}$-$\tilde{e}_R$-e_R vertex has a simple relation to the B-e-e coupling in the MSSM:

$$g_{\tilde{B}\tilde{e}_R e_R}=\sqrt{2}g\tan\theta_W=\sqrt{2}g'. \tag{19}$$

This relation is imposed by supersymmetry. Thus the measurement of $g_{\tilde{B}\tilde{e}e}$ will allow us to prove that $\tilde{e}$ and $\tilde{B}$ are indeed superpartners of e_R and B.

For this test we modify the relation of Eq. (19) as

$$g_{\tilde{B}\tilde{e}_R e_R}=\sqrt{2}g' Y_{\tilde{B}} \tag{20}$$

and estimate the sensitivity to $Y_{\tilde{B}}$ by introducing a new $\Delta\overline{\chi^2}$ function for the selectron pair production which depends on $Y_{\tilde{B}}$ though $g_{\tilde{B}\tilde{e}_R e}$. In the limit of $m_Z \ll M_1$ and μ, we obtain an approximate formula for the matrix element $\mathcal{M}$:

$$\mathcal{M}\propto \sin\theta\left[1-\frac{4Y_{\tilde{B}}^2}{1-2\cos\theta\beta_f+\beta_f^2+4M_1^2/s}\right]. \tag{21}$$

It is apparent from Eq. (21) that one can constrain both $Y_{\tilde{B}}$ and M_1 by measuring the differential cross section: $d\sigma(e^+e^-\to\tilde{e}_R^+\tilde{e}_R^-)/d\cos\theta$.

Figure 14 is a $\Delta\overline{\chi^2_{\tilde{e}}}$ contour plot projected on the M_1-$Y_{\tilde{B}}$ plane for a representative point in the parameter space of the MSSM: $m_{\tilde{e}_R}=200$ GeV, $\mu=300$ GeV, $M_1=99.57$ GeV, and tan$\beta=2$. One finds a good sensitivity to the coupling $Y_{\tilde{B}}$ of $\sim 1\%$ in this case. The reason why we got upper and lower bounds on M_1 and $Y_{\tilde{B}}$ is as follows: When we increase M_1' from M_1 to $M_1+\Delta M_1$, the total cross section decreases. The

[16]The direction of a produced chargino can be solved for with a twofold ambiguity when the chargino decays into $W\tilde{\chi}_1^0$ [6]. The forward-backward asymmetry for the final state W can also be used even if the $\tilde{\chi}_1^+$ decays into $W^*\tilde{\chi}_1^0$ [25,7].

[17]$\Delta m_{\tilde{\chi}_1^\pm}$ was found to be around 5% for 50 fb^{-1} of data [6]. A threshold scan for the $\tilde{\chi}_1^+\tilde{\chi}_1^-$ pair production might determine the mass better.

[18]It has been claimed that a very precise measurement of tanβ is possible when tan$\beta\sim 4$ [7] if the chargino mass errors are negligibly small. Some additional error on tanβ has been introduced here assuming a finite error on $m_{\chi_i^\pm}$. In Fig. 13, we have also taken a larger value of $m_{\tilde{\nu}}$ compared to [7], where sensitivity to tanβ is smaller.

corresponding increase of $\Delta\overline{\chi^2_{\tilde{e}}}$ can be compensated by increasing Y_B. However, because of the constraint on $m_{\tilde{\chi}^0_1}$ which comes from the electron energy distribution from decaying $\tilde{e}_R$'s, the optimized value of μ' is smaller for a larger M_1' (see Fig. 2 for the relation between M_1 and μ). Hence the second lightest neutralino mass is lighter for a larger M_1', and it also tends to have a larger mixing with $\tilde{B}$. At the M_1' upper bound of $\Delta\overline{\chi^2}=1$, the polar angle distribution changes its shape so that it is less forwardly peaked. On the other hand, the lower bound on M_1' is determined by $m_{\tilde{\chi}^0_1}$. Namely, for given M_1, there is a upper bound on $m_{\tilde{\chi}^0_1}$ which one can obtain by varying μ and $\tan\beta$ maximally. It becomes thus harder to reproduce the input $m_{\tilde{\chi}^0_1}$ as we decrease M_1'.

Some deviation of $Y_{\tilde{B}}$ from its tree-level value is expected if we take into account the effect of radiative corrections in the framework of the MSSM. If there is a large difference between several soft SUSY-breaking mass parameters, such a correction occurs very naturally. For example, if $m_{\tilde{q}} \gg m_{\tilde{l}}$ and $m_{\tilde{\chi}}$, the effective theory below $Q < m_{\tilde{q}}$ is not supersymmetric, and couplings related by supersymmetry start to run differently according to the RG equations of the effective theory. In particular, both squarks and quarks decouple from the wave function renormalizations of gauginos in the low energy effective theory, while only squarks decouple from that of gauge bosons, from which $Y_{\tilde{B}} \neq 1$ may originate.

The RG equations below the squark decoupling are [26]

$$\frac{d\alpha'}{d\ln Q} = \frac{55}{12\pi}\alpha'^2, \tag{22a}$$

$$\frac{d\alpha_{\tilde{B}\tilde{e}e}}{d\ln Q} = \frac{11}{4\pi}\alpha'\alpha_{\tilde{B}\tilde{e}e}, \tag{22b}$$

where we neglected terms proportional to $(Y_{\tilde{B}}-1)$ on the right-hand side of the equations. We find, from Eq. (22),

$$\Delta Y_{\tilde{B}e\tilde{e}}/Y_{\tilde{B}e\tilde{e}} = 0.007 t_{\tilde{q}\tilde{e}}, \tag{23}$$

where $t_{\tilde{q}\tilde{l}} = \log_{10}(m_{\tilde{q}}/m_{\tilde{l}})$.

It is rather striking that the error on the couping is of about the same order as that of the radiative correction proportional to $\log(m_{\tilde{q}}/m_{\tilde{l}})$ if the squark mass is much heavier than the slepton mass. This, on the one hand, requires knowledge of $m_{\tilde{q}}$ and a full one-loop calculation of the process to remove the uncertainty in $Y_{\tilde{B}}$ from the determination of M_1; notice that the error on M_1 increases by a factor of 2, if we let Y_B move freely. This also implies a larger error on $\tan\beta$, as the errors on M_1 and $\tan\beta$ are correlated strongly when the lightest neutralino is gaugino dominant. On the other hand, we can turn this argument around. Then emerges the possibility to constrain the squark mass scale from the measurement of $Y_{\tilde{B}}$ or other couplings even if the energy of future colliders is not enough for the squark production. A full calculation of one-loop radiative corrections to this process is eagerly anticipated.

A similar radiative correction to $g_{\tilde{W}\tilde{\nu}e_L}$ turns out to be of the order of $2\% \times \log_{10}(m_{\tilde{q}}/m_{\tilde{l}})$, but the sensitivity to this coupling has been argued to be rather poor [7]: about $-15\%+30\%$ for a representative parameter choice. This estimate is based on the study of gaugino-dominant chargino production and decay, using the forward-backward asymmetry of the decay products and the total production cross section. The chargino production proceeds through t-channel exchange of $\tilde{\nu}$, and the $\tilde{\nu}$ is assumed to be kinematically inaccessible in the study. Its mass is determined by comparing the production cross sections for polarized and unpolarized electron beams, and the decay forward-backward asymmetry, but it has a very large uncertainty. Furthermore, the uncertainty in the branching ratios introduces a systematic error to the measurement of the total cross section. Notice that the production cross section of gaugino-dominant charginos is very small for a right-handed polarized beam; hence, the chargino study heavily relies on the use of the unpolarized beam; where large backgrounds limit the decay modes to study. The estimated error in the cross section is about 5% for $\int \mathcal{L}dt = 100$ fb^{-1}. These uncertainties limited the $g_{\tilde{W}\tilde{\nu}e}$ study.[19]

The coupling $g_{\tilde{B}\tilde{e}_R e}$ is considerably easier to measure than $g_{\tilde{W}\tilde{\nu}e}$. $\tilde{e}_R$ has a sizable production cross section for the right-handed electron beam, and the uncertainty in the production cross section is expected to be very small if the $\tilde{e}$ decays exclusively into $e\tilde{\chi}^0_1$. For the representative parameters of Fig. 14, the t-channel exchange of neutralinos is dominated by the lightest one, $\tilde{\chi}^0_1$, and its mass is well constrained from the $\tilde{e}_R$ decay data. It is therefore not surprising that the coupling is measured very well here.

Deviations from tree-level MSSM predictions can also appear in other couplings involving sleptons or neutralinos, such as $g_{\tilde{H}l\tilde{l}}$. Unfortunately, the measurement of $\tan\beta$ has a large error; thus, radiative corrections may not be relevant in this case. The gaugino mass matrix also gets radiative corrections to its tree-level value [28]. If one assumes a unified gaugino mass at the GUT scale, one may in principle extract the squark mass scale from the gaugino mass relation at the weak scale. Unfortunately, the measurements of gaugino masses are limited by ambiguities in the neutralino and chargino mixing angles [5–7]. The gluino mass, though involving no mixing, is hard to measure precisely at hadron colliders, too [29].

Now we turn our attention to $\tilde{\tau}_1$ production. In the previous subsection, we found that $P_\tau(\tilde{\tau}_1 \to \tau\tilde{\chi}^0_1)$ becomes independent of $\tan\beta$, if $\tilde{\chi}^0_1$ is gaugino dominant, or in other words $m_{\tilde{\chi}^0_1} \sim M_1$. In such a situation, simultaneous measurements of $\theta_{\tilde{\tau}}$ (using the total $\tilde{\tau}_1$-pair production cross section) and P_τ constrain the nature of the $\tilde{B}$-$\tilde{\tau}$-τ coupling instead of constraining $\tan\beta$. Given the fact that $\tilde{\chi}^0_1$ is almost a pure gaugino (which can be checked with scalar electron production), the measurement of the total $\tilde{\tau}_1$ pair production cross section essentially fixes the polarization P_τ through Eq. (8). Any deviation of P_τ from it indicates that something unexpected is happening.

In Fig. 15 we show $\Delta\overline{\chi^2}=1$ contours by taking the mixing angle parameter ($\theta_{\tilde{\tau}}$) in the $\tilde{\chi}\tilde{\tau}\tau$ coupling free from that

[19] During this work, we learned of similar work on measuring decoupling effects by Cheng, Feng, and Polonsky [27]. We thank Jonathan Feng for bringing this work to our attention.

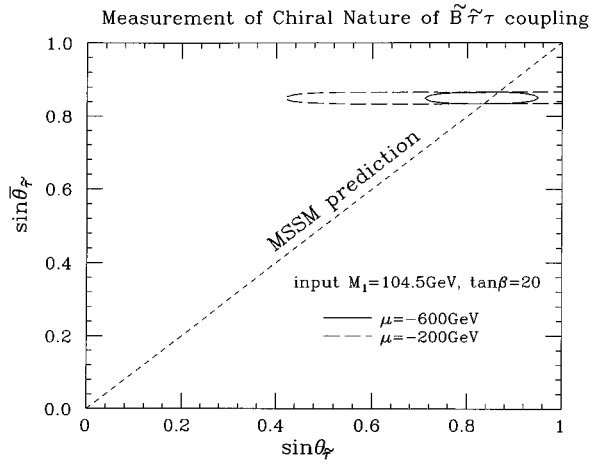

FIG. 15. $\Delta\chi^2=1$ contours when the mixing angle $\theta_{\tilde{\tau}}$ in the $\tilde{\chi}_1^0\tilde{\tau}\tau$ is allowed to move freely from that in the $Z\tilde{\tau}\tau$ coupling ($\bar{\theta}_{\tilde{\tau}}$). $\theta_{\tilde{\tau}}-\bar{\theta}_{\tilde{\tau}}$ parametrizes the chirality flipping part of the $\tilde{B}(\tilde{W})$-$\tilde{\tau}$-τ interaction, which is zero in the MSSM. The solid line corresponds to $\mu=-600$ GeV and the dashed line to $\mu=-200$ GeV. The other parameters are fixed to $M_1=104.5$ GeV and $\tan\beta=20$. The sensitivity is moderate for $\mu\gg M_1$.

in the $Z\tilde{\tau}\tilde{\tau}$ coupling ($\bar{\theta}_{\tilde{\tau}}$). We can say that $\theta_{\tilde{\tau}}-\bar{\theta}_{\tilde{\tau}}$ measures the chirality flipping part of the $\tilde{B}(\tilde{W})$-$\tilde{\tau}$-τ interaction which is zero in the MSSM. Because of the dependence of P_τ on $\tan\beta$ through a small but finite Higgsino component in the neutralino mass eigenstate ($\tilde{\chi}_1^0$), the sensitivity of the $\tilde{\tau}\tau\tilde{\chi}_1^0$ coupling to the $\theta_{\tilde{\tau}}$ is marginal[20] unless $\mu\gg M_1$.

Nevertheless, the figure can be regarded as an example of a ''no lose theorem'' of precision measurements of supersymmetry processes. Depending on the position in the parameter space of the model, we occasionally lose sensitivity to some parameter, as we have seen for the $\tan\beta$ determination using slepton production. We can, however, turn this into an advantage: The process becomes independent of the ambiguity caused by the parameter, and we can test its supersymmetric nature. In the current case, we can check the chiral nature of the gaugino, thanks to the insensitivity of the process to $\tan\beta$.

V. CONCLUSION

In this paper we presented an extensive study of the production of the lighter scalar τ lepton $\tilde{\tau}_1$ and its decay into the lightest neutralino χ_1^0 and τ at a future LC. We also discussed physics that could be extracted from them. Studying $\tilde{\tau}$ production is important because it may be lighter than the other sleptons and could thus be found earlier. The light $\tilde{\tau}_1$ case is also theoretically well motivated in the MSUGRA-GUT model and is not excluded, at least, in other models, as long as there is a large $\tilde{\tau}_L$-$\tilde{\tau}_R$ mixing.

We discussed that the $\tilde{\tau}$ mass matrix at $M_{\rm GUT}$ might provide a clue to distinguishing SUGRA-GUT from DNNS models. In order to obtain the GUT scale mass matrix, one must know the mass matrix at the weak scale and the τ Yukawa coupling (Y_τ) which is characterized by $\tan\beta$.

The mass matrix can be determined if one knows the $\tilde{\tau}$ masses and mixing angle $\theta_{\tilde{\tau}}$. The feasibility of determining those parameters at a LC has been studied for the lighter mass eigenstate $\tilde{\tau}_1$, assuming the JLC1 model detector. For a representative parameter set $m_{\tilde{\tau}_1}=150$ GeV and $m_{\tilde{\chi}_1^0}=100$ GeV, we found that these masses can be measured to $\Delta m_{\tilde{\tau}_1}=4.1$ GeV and $\Delta m_{\tilde{\chi}_1^0}=3$ GeV for 10^4 $\tilde{\tau}_1$ pairs produced with a background corresponding to $\int\mathcal{L}dt=100$ fb^{-1}, assuming that $\tilde{\tau}_1$'s decay exclusively into $\tilde{\chi}_1^0\tau$. For the same mass parameters and luminosity conditions, the expected statistical error on the mixing angle turned out to be $\Delta\sin\theta_{\tilde{\tau}}=0.045$, when $\sin\theta_{\tilde{\tau}}=0.75$.

The polarization (P_τ) of τ leptons from $\tilde{\tau}_1$ decay is sensitive to $\tan\beta$ because of its dependence on the τ Yukawa coupling. The expected statistical error in the polarization was estimated to be ±0.07 for 10^4 $\tilde{\tau}_1$ pairs and background corresponding to $\int\mathcal{L}dt=100$ fb^{-1}. Using the information of the neutralino mass matrix obtained from the simultaneous studies of the $\tilde{e}_R$ production and decay, $\tan\beta$ might be determined. The error in $\tan\beta$ varies drastically with M_1 and $m_{\tilde{\chi}_1^0}$, as shown in Fig. 12 for some representative points in the parameter space of the MSSM.

Notice that $\tan\beta$ is one of the most important parameters that determine the Higgs sector of the MSSM. At the same time, it is known to be difficult to measure especially if it is large. If $\tan\beta>10$, $\tilde{\tau}_1$ decays give us a unique opportunity to determine $\tan\beta$.

We have also discussed a possibility to test the supersymmetry relations among couplings involving superpartners. By studying the polar angle distribution of $\tilde{e}_R$ production, one can measure not only M_1, $m_{\tilde{\chi}_1^0}$, but also the gaugino-selectron-electron coupling $g_{\tilde{B}\tilde{e}_R e}$. A fit allowing $g_{\tilde{B}\tilde{e}_R e}$ to move freely from the tree-level prediction of supersymmetry gives $\Delta g_{\tilde{B}\tilde{e}_R e}\sim1\%$–$2\%$. This is comparable to typical radiative corrections to the same coupling $\sim0.7\%\times\log_{10}(m_{\tilde{q}}/m_{\tilde{l}})$. This suggests that the LC might allow us to start probing radiative corrections to couplings involving SUSY particles.

Implications of the MSUGRA model at the CERN e^+e^- collider (LEP II) and Large Hadron Collider (LHC) have been discussed and studied in many papers. Unfortunately, prospects to determine the soft SUSY-breaking mass parameters are not so bright there: As for LEP II, its available luminosity is too low for the slepton study and one has to fight the enormous background coming from W^+W^- production for chargino study [25], while at LHC, one suffers from the high QCD background even though strongly interacting superparticles will be copiously produced. Therefore those studies in the framework of the MSUGRA model are focused mostly on the discovery potential of the machine in question [30]. However, it is becoming more and more recognized that we can certainly go beyond that if a next generation linear e^+e^- collider is actually built. Namely, the experiments at the LC will make it possible to measure the parameters of the MSSM once a superparticle is discovered, which will then enable us to check the predictions of the models of SUSY breaking.

[20]The contours in Fig. 15 depend sensitively on the region of $\tan\beta$ searched. We took $1<\tan\beta<50$ here to obtain $\Delta\chi^2=1$, assuming that the Yukawa coupling is not too large at the GUT scale.

ACKNOWLEDGMENTS

One of the authors (M.M.N.) has benefited from an unfinished collaboration with J. Hisano and Y. Yamada. The authors are grateful to M. Tanaka for checking the $e^+e^-\tau^+\tau^-$ background cross section independently. The authors also thank M. Drees and K. Hikasa for reading the manuscript carefully. This work was supported in part by a Grant in aid for Science and Culture of Japan (No. 07640428).

APPENDIX A: PARAMETERS OF THE MSSM

In this subsection, we are going to summarize the interactions of $\tilde{\tau}$ that are relevant for the analysis in this paper. The interactions are fixed by supersymmetry and gauge symmetry, as well as by the mass parameters of the model.

The $\tilde{\tau}$-τ-gaugino interactions relevant to $\tilde{\tau}_i$ decay are expressed by the Lagrangian [12]

$$\mathcal{L}=\sum_{i=1,2\ j=1,\ldots,4}\tilde{\tau}_i\overline{\tau}(P_L a_{ij}^R+P_R a_{ij}^L)\tilde{\chi}_j^0 + \sum_{i=1,2\ j=1,2}\tilde{\tau}_i\overline{\nu_\tau}P_R b_{ij}\tilde{\chi}_j^+ + \text{H.c.}, \tag{A1}$$

where

$$\begin{pmatrix} a_{1j}^{R(L)} \\ a_{2j}^{R(L)} \end{pmatrix}=\begin{pmatrix} \cos\theta_{\tilde{\tau}} & \sin\theta_{\tilde{\tau}} \\ -\sin\theta_{\tilde{\tau}} & \cos\theta_{\tilde{\tau}} \end{pmatrix}\begin{pmatrix} a_{Lj}^{R(L)} \\ a_{Rj}^{R(L)} \end{pmatrix},$$

$$\begin{pmatrix} b_{1j} \\ b_{2j} \end{pmatrix}=\begin{pmatrix} \cos\theta_{\tilde{\tau}} & \sin\theta_{\tilde{\tau}} \\ -\sin\theta_{\tilde{\tau}} & \cos\theta_{\tilde{\tau}} \end{pmatrix}\begin{pmatrix} b_{Lj} \\ b_{Rj} \end{pmatrix}, \tag{A2a}$$

$$a_{Lj}^R=-\frac{gm_\tau}{\sqrt{2}m_W\cos\beta}N_{j3},\quad a_{Lj}^L=\frac{g}{\sqrt{2}}[N_{j2}+N_{j1}\tan\theta_W],$$

$$a_{Rj}^R=-\frac{2g}{\sqrt{2}}N_{j1}\tan\theta_W,\quad a_{Rj}^L=-\frac{gm_\tau}{\sqrt{2}m_W\cos\beta}N_{j3},$$

$$b_{Lj}=-gU_{j1},\quad b_{Rj}=\frac{gm_\tau}{\sqrt{2}m_W\cos\beta}U_{j2}. \tag{A2b}$$

Here the real orthogonal matrix N_{ij} and unitary matrices U_{ij} and V_{ij} are the diagonalization matrices of the neutralino mass matrix $\mathcal{M}_N$ and chargino mass matrix $\mathcal{M}_C$ as follows:

$$U^*\mathcal{M}_C V^{-1}=M_C^D,\quad N\mathcal{M}_N N^{-1}=M_N^D, \tag{A3}$$

where the mass matrices are written in the form

$$\mathcal{M}_N(\tilde{B},\tilde{W}_3,\tilde{H}_1,\tilde{H}_2)=\begin{pmatrix} M_1 & 0 & -m_Z\sin\theta_W\cos\beta & m_Z\sin\theta_W\sin\beta \\ 0 & M_2 & m_Z\cos\theta_W\cos\beta & -m_Z\cos\theta_W\sin\beta \\ -m_Z\sin\theta_W\cos\beta & m_Z\cos\theta_W\cos\beta & 0 & -\mu \\ m_Z\sin\theta_W\sin\beta & -m_Z\cos\theta_W\sin\beta & -\mu & 0 \end{pmatrix}, \tag{A4a}$$

$$\mathcal{M}_C(\tilde{W},\tilde{H})=\begin{pmatrix} M_2 & m_W\sqrt{2}\sin\beta \\ m_W\sqrt{2}\cos\beta & \mu \end{pmatrix}. \tag{A4b}$$

μ is a supersymmetric Higgsino mass parameter, while M_1 and M_2 are the soft breaking mass parameters of B-ino and W-ino introduced previously. The mass eigenstate $\tilde{\chi}_i^0$ and current eigenstates $\tilde{B},\tilde{W},\tilde{H}_1,\tilde{H}_2$ are related by

$$\tilde{\chi}_i^0=N_{i1}\tilde{B}+N_{i2}\tilde{W}+N_{i3}\tilde{H}_1+N_{i4}\tilde{H}_2. \tag{A5}$$

Unlike the notation of Haber and Kane [1], we take N to be real so that $m_{\tilde{\chi}_i^0}$ can be either positive or negative. Its sign must be kept to understand the equations in Ref. [12]. We take $|m_{\tilde{\chi}_1^0}|\leqslant|m_{\tilde{\chi}_2^0}|\leqslant|m_{\tilde{\chi}_3^0}|\leqslant|m_{\tilde{\chi}_4^0}|$ and $0\leqslant m_{\tilde{\chi}_1^-}\leqslant m_{\tilde{\chi}_2^-}$. We assume the mass relation of MSUGRA $M_1=(5/3)\tan^2\theta_W M_2$ for numerical calculations in order to reduce the number of parameters.

Equation (A1) leads to an expression for P_τ:

$$P_\tau(\tilde{\tau}_1\to\tilde{\chi}_1^0\tau)=\frac{(a_{11}^R)^2-(a_{11}^L)^2}{(a_{11}^R)^2+(a_{11}^L)^2}. \tag{A6}$$

APPENDIX B: $\tilde{e}_R$ PRODUCTION

$\tilde{e}_R$ production proceeds through t-channel exchange of neutralinos and s-channel exchange of gauge bosons. The tree-level couplings of the $\tilde{e}_R e\tilde{\chi}_i^0$ vertices may be read off from Eqs. (A1) and (A2) by setting $\sin\theta_{\tilde{\tau}}=1$ and replacing $\tau\to e$. We obtain the formula for the $\tilde{e}_R$-pair production cross section as

$$\frac{d\sigma}{d\cos\theta}(h_e,\overline{h_e})=\frac{1}{2s}\frac{\beta_f}{16\pi}\frac{1}{2}\sum_{h_e}|\mathcal{M}(h_e,\overline{h_e})|^2, \tag{B1a}$$

$$i\mathcal{M}(h_e,\overline{h_e})=-i\lambda_i e^{i\lambda_i\phi}\sin\theta s\beta_f\left[g_Z^2\frac{A_{h_e}A_{1/2}}{s-m_Z^2+i\Gamma_Z}+\frac{e^2}{s}+\frac{1\pm(-)^{\overline{h+1/2}}}{2}\sum_j\frac{1}{2}\frac{A_{jR}^2}{t-m_{\tilde{\chi}_j}^2}\right], \tag{B1b}$$

where $h_e(\overline{h_e})=\pm1/2$ represents the helicity of the initial-state electron (positron), $\lambda_i\equiv h_e-\overline{h_e}$, θ and β_f are the $\tilde{e}_R^-$ production angle and velocity, and $t=(-s/4)(1-2\cos\theta\beta_f+\beta_f^2)$. The couplings A_{h_e} and $A_{jR(L)}$ are given by

$$A_{1/2}=\sin^2\theta_W,\quad A_{-1/2}=-\tfrac{1}{2}+\sin^2\theta_W$$

$$A_{jR}=-\sqrt{2}g\tan\theta_W N_{j1}. \tag{B2}$$

[1] For reviews, see H. E. Haber and G. L. Kane, Phys. Rep. **117**, 75 (1985).
[2] U. Amaldi, W. de Boer, and H. Fürstenau, Phys. Lett. B **260**, 447 (1991); P. Langacker and M. Luo, Phys. Rev. D **44**, 817 (1991); J. Ellis, S. Kelley, and D. V. Nanopoulos, Phys. Rev. B **260**, 131 (1991).
[3] For reviews, see H. P. Nilles, Phys. Rep. **110**, 1 (1984).
[4] M. Dine, A. E. Nelson, Y. Nir, and Y. Shirman, Phys. Rev. D **53**, 2658 (1996).
[5] ''JLC I,'' KEK Report No. 92-16 (unpublished).
[6] T. Tsukamoto *et al.*, Phys. Rev. D **51**, 3153 (1995).
[7] J. L. Feng *et al.*, Phys. Rev. D **52**, 1418 (1995).
[8] Contributions at the workshop on ''Physics and Experiments with Linear e^+e^- Colliders'' at Morioka-Appi, Iwate, Japan, 1995 (unpublished): See also *Proceedings of Workshop on Physics and Experiments with Linear e^+e^- Colliders*, Waikoloa, Hawaii, 1993, edited by F. A. Harris *et al.* (World Scientific, Singapore, 1993).
[9] *e^+e^- Collisions at 500 GeV: The Physics Potential*, Proceedings of the Workshop, Munich, Annecy, France, 1991, edited by P. M. Zerwas (DESY Report No. 92-123A,B,C, Hamburg, 1992), and references therein.
[10] R. Barbieri and L. J. Hall, Phys. Lett. B **338**, 212 (1994); R. Barbieri, L. Hall, and A. Strumia, Nucl. Phys. **B445**, 219 (1995).
[11] B. Ananthannarayan, G. Lazarides, and Q. Shafi, Phys. Rev. D **44**, 1613 (1991); S. Kelley, J. L. Lopez, and D. V. Nanopoulos, Phys. Lett. B **274**, 387 (1992).
[12] M. M. Nojiri, Phys. Rev. D **51**, 6281 (1995).
[13] Mihoko M. Nojiri, presented at the the 5th Workshop on JLC, Kawatabi, Japan (unpublished), Report No. hep-ph/9504890 (unpublished); K. Fujii, M. M. Nojiri, and T. Tsukamoto, presented at Yukawa International Symposium, Kyoto, Japan (unpublished), Report No. hep-ph/9511338 (unpublished).
[14] B. K. Bullock, K. Hagiwara, and A. D. Martine, Phys. Rev. Lett. **67**, 3055 (1991); D. P. Roy, Phys. Lett. B **277**, 183 (1992).
[15] R. Rattazzi, U. Sarid, and L. J. Hall, ''Yukawa Unification: The Good, The Bad, and The Ugly,'' Report No. SU-ITP-94-15, hep-ph/9405313 (unpublished).
[16] M. Drees and M. M. Nojiri, Nucl. Phys. **B369**, 54 (1992).
[17] J. A. Casas, A. Lleyda, and C. M̃unoz, Nucl. Phys. **B471**, 1 (1996).
[18] Y. S. Tsai, Phys. Rev. D **4**, 2821 (1971); T. Hagiwara, S.-Y. Pi, and A. I. Sanda, Ann. Phys. (N.Y.) **106**, 134 (1977); A. Rougé, Z. Phys. C **48**, 75 (1990); H. Kühn and F. Wagner, Nucl. Phys. **B236**, 16 (1984); See also B. K. Bullock, K. Hagiwara, and A. D. Martin, *ibid.* **B395**, 499 (1993).
[19] H. Murayama, I. Watanabe, and K. Hagiwara, KEK Report No. 91-11, 1992 (unpublished).
[20] S. Kawabata, Comput. Phys. Commun. **41**, 127 (1986).
[21] S. Jadach and J. H. Kühn, Comput. Phys. Commun. **64**, 275 (1991); M. Jeżabek, Z. Wąs, S. Jadach, and J. H. Kühn, *ibid.* **70**, 69 (1992); **76**, 361 (1993).
[22] K. Fujii, T. Matsui, and Y. Sumino, Phys. Rev. D **50**, 4341 (1994).
[23] M. Kuroda, Meiji Gaikuin University Report No. MGU-DP 7, 1988 (unpublished); M. Kuroda, Meiji Gaikuin Univ. (Tokyo), Res. J. **424**, 27 (1988).
[24] K. Fujii (private communication).
[25] J. L. Feng and M. J. Strassler, Phys. Rev. D **51**, 4661 (1995).
[26] P. H. Chankowski, Phys. Rev. D **41**, 2877 (1990).
[27] H.-C. Cheng, J. L. Feng, and N. Polonksy (in preparation).
[28] S. Martin and M. Vaughn, Phys. Rev. D **50**, 2282 (1994); D. Pierce and A. Papadopoulous, Nucl. Phys. **B430**, 278 (1994); N. V. Krasnikov, Phys. Lett. B **345**, 25 (1995); D. Pierce and A. Papadopoulos, Phys. Rev. D **50**, 565 (1994).
[29] R. M. Barnett, J. Gunion, and H. Haber, Phys. Lett. B **315**, 349 (1993); H. Baer, C. H. Chen, F. Paige, and X. Tata, Phys. Rev. D **52**, 2746 (1995).
[30] In recent snowmass studies, it has been shown that LHC can measure mass differences of some SUSY particles rather accurately for some MSUGRA points. See, for example, F. E. Paige, ''Determining SUSY Particle Masses at LHC,'' Report No. hep-ph/9609373 (unpublished).